Doctoral Dissertation

Fatigue Fracture Properties of Nanoclay and Wood Plastic Composites

September, 2015

MOHD NUR AZMI BIN NORDIN

Graduate School of Science and Engineering,
Yamaguchi University

Table of Contents

Nomenclature

CMCs	Ceramic matrix composites
MMCs	Metal matrix composites
PMCs	Polymer matrix composites
FRP	Fiber reinforced plastic
UD	Unidirectional
XRD	X-ray diffraction
TEM	Transmission electron micrographic
WAXD	Wide angle X-ray diffraction
SEM	Scanning electron microscopy
EPMA	Electron probe micro-analyzer
WPCs	Wood-plastic composites
PP	Polypropylene
NE-	Nanoclay-epoxy
MAPP	Maleic anhydride polypropylene
S-N	Stress to the number of cycles to fracture
MDF	Medium density fiberboard
MA	Maleic anhydride
AA	Acrylic acid
MFI	Melt flow index

Symbols and Units

F_{ci}	Fatigue fracture surface at crack initiation area
F_{pi}	Fatigue fracture surface at peak intensity area
G(R)	nearest neighbor function
R	radius from nanoclay agglomerate's centroid
d_i	nearest neighbor distance
rpm	rotation per minute
phr	parts per hundred parts of resin
wt.%	percentage of weight (mass) fraction
°C	degree Celsius
h	hour(s)

Chapter I General Introduction

1.1 Background

Development of new advanced materials due the needs from the industries has placed a number of conditions such as light in weight, high durability and low production cost as a minimum prerequisite that are necessary to be full filled. The production of composite materials for example has put these elements as a main goal that is by combining two or more materials with different properties in order to give a performance in service which is superior to the properties of the individual materials. The composite materials have been used over centuries as construction materials - ancient Egyptians mixed the wheat straws with the Nil's mud to make bricks for their house, where the straws functioned as reinforcement to the mud to make the bricks strong, besides keep the house cool when it is hot in summer and vice versa. The implementation of the *'combining materials'* idea bring interest to many people from various fields over the time until recent, which is known as a composite materials in the present-day. Fig. 1.1 illustrates the schematic of reinforcing and binding elements of composite materials. It is commonly use in many applications such as aerospace industry, where the high thermal shock resistance and excellent fracture toughness of ceramic matrix composites (CMCs) material is applied for heat shield of the space vehicles, and also widely applied in automotives and as a material for sports equipments due to its light weight, tremendous elasticity and strength. Metal matrix composites (MMCs) are practically used for vehicle parts such as engine, rotors and disc brakes; because of relatively high thermal properties of the composite materials, and also commonly applied as a structure frames for many sports applications such as bicycles, rackets and as well as golf shafts.

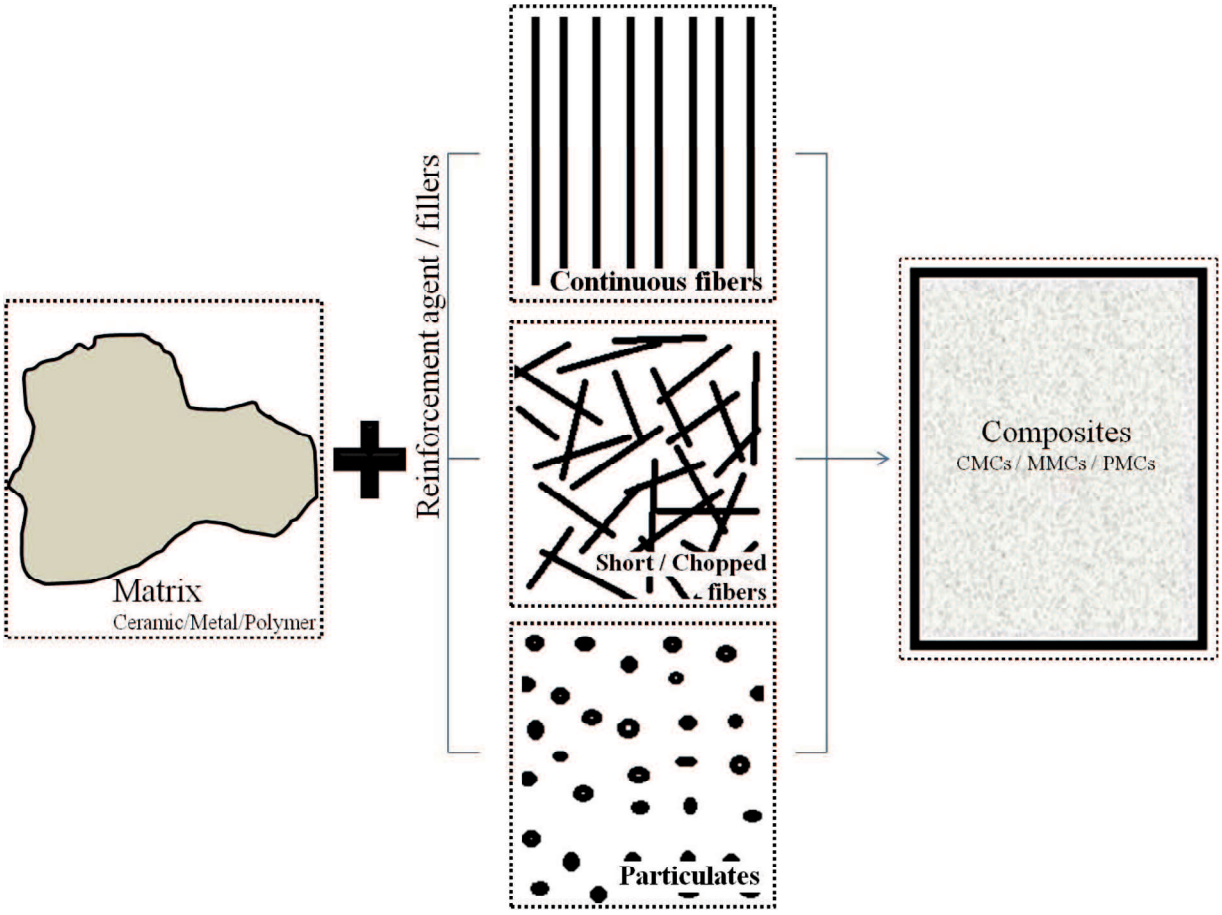

Fig. 1.1 Schematic of composites elements.

Composite materials are designed to suit its properties to a certain application in order to optimize the consumption of the raw materials while giving a maximum performance. Similar to the other types of composites stated above, polymer matrix composites (PMCs) is applied to a certain parts of products in which appropriate with its range of properties and performances such as the interior and exterior parts of the vehicles, containers and also as a building panels. Over decades, numerous studies on PMCs properties as well as the development of new type of PMCs had been carried out. Fiber reinforced plastic (FRP) composites, for instance, gain interest from both manufacturers and researcher on improving the bulk properties of the materials to maximize the overall performances regarding to the applied field. Consequently, the FRP materials show

higher modulus per unit weight, *specific modulus* and strength per unit weight, *specific strength* when compared to other metal or monolithic materials, i.e., imply the weight savings over the whole structure, thus resulted in greater efficiency and energy savings to the outcome of the composites products. Plastic is defined as a polymeric material that formed by large molecules that are composed of many (*poly*-) repeats of simpler structural unit, the *mer*, connected by covalent chemical bonds. There are two types of polymeric plastic regarding to the engineering materials definition; thermosets and thermoplastics [1]. Thermosets are low-molecular-weight polymer that formed a cross-linked structure from the chemical reactions driven by the heating that is generated either by the reactions or from the external supplied heat. In opposites, thermoplastics are high-molecular-weight polymer that held together by weak secondary bonding. The cross-linking reaction does not formed in the thermoplastics as thermosets does, however, they can be reprocessed. The weak secondary bonds break down when high temperature is applied and reform during the cooling process. The differences between thermosets and thermoplastics were summarized as shown in Table 1.1. It is known that the virgin plastic or the pure polymeric materials have low in strength and stiffness properties; moreover, most are less resistance towards high temperature, which make it difficult to be applied individually in many engineering applications. Making the polymeric plastic as the binding constituent of composite materials, thus, by incorporating the fillers like fibers or particulates into the matrix, the mechanical and thermal properties of the plastic materials indicated an excellent improvements [2-5,20] despites several difficulties such as poor distribution and lack in interfacial adhesion between the fillers and the matrix, that need to be encountered. In this study, the PMCs were chosen as the subject material that would be varied by the difference of reinforcement fillers,

Table 1.1 General characteristics of thermosets and thermoplastics. Source:[1]

Thermoplastics	Thermosets
high molecular weight and high viscosity	low molecular weight and low viscosity monomers
do not form cross-linking reactions	cross-linked structures are generated from the chemical reactions that are driven by heat
able to reprocessed	cannot be re-melted
either amorphous or semicrystalline structure	amorphous structure; brittle

where the performances of these different PMCs material were measured and evaluated through their reliability from the mechanical behavior.

The reinforcement agent or fillers in composite materials plays an important role in order to hold the matrix that is by transferring the load and act as a *crack-bridge* at a crack tip upon failure. Fig. 1.2 indicates several examples of reinforcements that are commonly used for composite materials. The compatibility of fillers with the matrices has put extra advantageous for composites to uphold the local area towards given loads and therefore enhanced the performance of the overall composite materials. There are several types of fillers depends on the (i) structure or geometrical shapes, (ii) size and (iii) origin of the fillers.

i. **Structure or geometrical shapes** - Unidirectional (UD) fiber is commonly used as reinforcement agent in many composite materials. It may be includes under the continuous fiber type that provides strong strengthening result to the matrix, and may stacked together of different layers and directions to form a laminae structure. The laminae structure also may consist of woven roving of continuous fiber or a

mix of aligned unidirectional layer with random short fibers including chopped fibers or whiskers. High stiffness of particulates fillers of various geometrical shapes such as spheres, plates, ellipsoids or hollow, are often used as fillers to obtain a micro- or nano-size effect which offers an excellent improvements of composites properties.

ii. **Size** - The order of the size of fillers that is from nano- to micron-size, gives variety in results on the performance of the composite materials. The improvement of the composite materials properties can be achieved by the addition of low amounts of well dispersed small size fillers, in which a higher interfacial surface area results from an increased aspect ratio or surface–volume ratio of the fillers. Therefore, for example, the required amount of nano-size fillers is much lower than that of conventional micro-order fillers, such as ceramic particles and short fibers, in order to maximize the properties of the composites which also bring along the economic benefits.

iii. **Origin** - Generally, fillers can be differentiate from its material such as the glass, carbon, boron fibers or the fibers that originated from the plants or animal, which is namely as the natural-based fibers. The use of natural-based fibers had been practically used in PMCs type composites over years and increasingly due to the awareness of the environmental problems. Commonly, the waste from the forestry or agriculture were processed as a fillers of PMCs which bring lessen to the used of petroleum-based matrices while optimizing the natural resources.

Fig. 1.2 Different types of reinforcements applicable to fabricate composite materials.

1.1.1 Polymer nanocomposites

Polymer nanocomposite is a combination of nano-size stiff fillers with the polymer plastic matrix. The nano-size fillers can be defined as the particle that has at least one dimension in nanometer scale. The incorporation of nano-size fillers into plastic polymer or rubber creates a new class of material with an outstanding performance in functional properties such as gas barrier, as well as mechanical and thermal ones [3-5]. From the end of the last century, nanocomposite materials have been attracting a great attention to industrial sectors and academic researchers, who focus on the broad possibility of nano-size fillers compared to micro-size ones. As mentioned above, there is an economical point such that the required amount of nano-size fillers is lower than the conventional micro-order fillers, i.e. ceramic particles, short fibers, and many more. Moreover, great attentions to the nano-size fillers emerged for several other reasons including [6, 7]:

i. The fillers usually have different properties from bulk properties of the same materials;
ii. The fillers are small defect compared to micro-size fillers which are similar in size to the critical crack size, and this will cause a premature crack;
iii. Due to larger surface area of fillers, nanocomposites have a large volume of interfacial matrix material with properties.

However, insufficient dispersion of nano-size fillers in polymeric matrices brings less mechanical properties [4, 8] because of the fillers often form micron-size agglomerates. The portion that is containing more agglomerated fillers tends to impart higher stress concentration on polymeric matrix than the other parts. This reaction leads to a crack formation and thus reduces the potential of the polymer nanocomposite materials. Consequently, there are many

factors that contribute to the insufficient dispersion that affect the properties of the nanocomposites, such as the synthesis methods during the fabrication process, the types of nano-particles that been used and also the characteristics of polymer matrix, where it is compatible or not with the compounded fillers.

The dispersion of fillers in polymer commonly tends to become partially exfoliated and intercalated clusters, where the fillers are homogeneously distributed. The distribution states have been verified through an X-ray Diffraction (XRD) method analysis or with high resolution observation by using transmission electron micrographic (TEM) [5, 9]. As concern by many in this field, however, it is almost difficult to achieve a fully exfoliated state only by a single physical process. We need to take into account the other factors such as chemical modification of nano-size particles that might influence appropriate formation for the internal microstructure of the polymer nanocomposites. Evaluation on dispersion order of nanoclay particles commonly has been done through a qualitative analysis of which the nanocomposites' structure can simply be done using a wide angle X-ray diffraction (WAXD) analysis, scanning electron microscopy (SEM) or TEM observation.

1.1.2 Wood-Plastic Composites (WPCs)

Current issues on composite materials have been discussed and published in many literatures, including some virtuous inventions on improvement of mechanical properties and hybridizing conventional composites with bio-based fillers. This work includes the development of woods as reinforcing fillers for polymeric matrix to form an environmentally friendly composite material. Wood materials have been used in many products such as household articles, furniture and other interior items. The combination of wood flour with polymeric matrices, so-called as wood-polymer composites (WPCs), brings a new sight in wood-based application, i.e. high durability and excellent mechanical properties such as high tensile strength and stiffness [10-12] and low density. As fillers, these natural particles play a role of transferring the load and act as a *crack-bridge* at a crack tip upon failure. However due to the incompatibility of wood surface structure with the polymer matrix, the maximum performances of compounded wood particles in the composite materials are difficult to achieve. Fig. 1.3 illustrates the role of

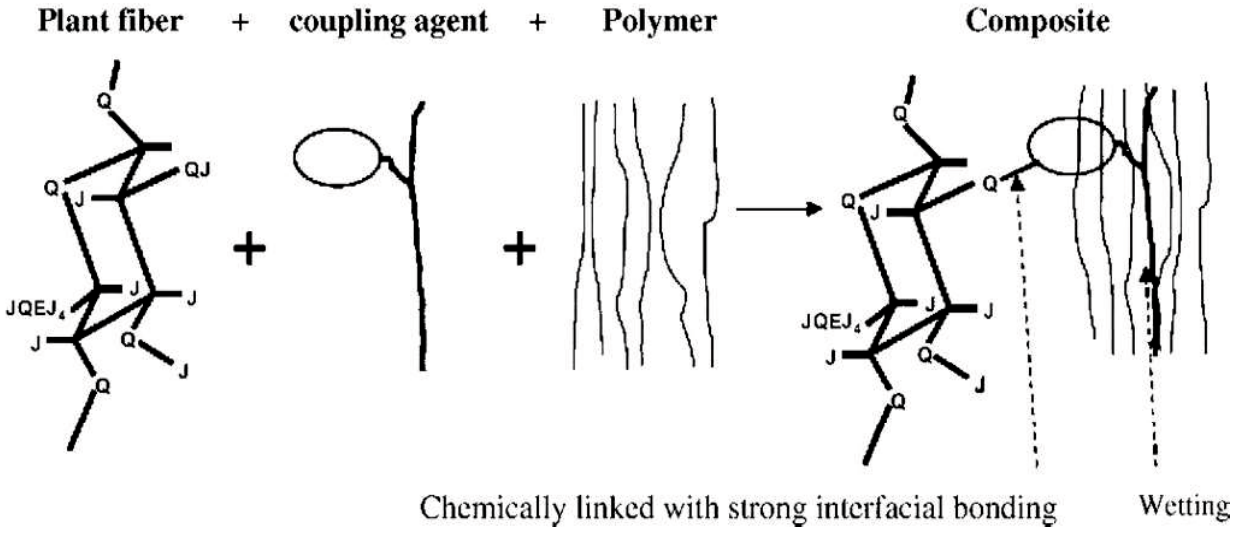

Fig. 1.3 Schematic figure of the mechanism of coupling agent between hydrophilic fiber and hydrophobic matrix polymer . Source [13].

coupling agent / compatibilizer in WPCs material. Moreover, the characteristics of wood flour are different with respect to the type of trees and harvesting time and it is easily influenced by the presence of moisture.

Another factor that contributes to the performance of WPCs material is the distribution of wood flour, i.e. the optimal amount of wood flour creates an appropriate condition for the fillers to transfer the loads and avoids the formation of wood cluster due to the lack of mixing process during the fabrication of WPCs. A study by Leu et al. [14] offers an idea of the optimization of wood fillers and other material composition in WPCs that helps to achieve ideal properties of the material. It is stated that by compounding up to 50 wt.% with the maximum value of coupling agent, *maleic anhydride polypropylene* (MAPP) at 3 wt.% able to enhanced the mechanical properties of WPCs. However, less data can be achieved regarding to the fatigue properties of the WPCs materials, which is highly recommended to be clarified. This is because the fatigue behaviors of WPCs material are important to estimate the life span or durability of the WPCs since the material itself has large potential to be applied in many applications. For an example, according to the fatigue behavior of natural fiber, Dijan et al. [15] suggested that high loading frequency reduced fatigue life of coir fiber reinforced polypropylene composites due to higher heat generation and less time available to dissipate the heat. This study imply the effect of heat that generated from loading and unloading actions, which is considerably close to the real applications, i.e. different loading frequency take place will results in heating and softening effects of the polymeric resin. Here, by understanding the fatigue behavior of WPCs material helps to contribute to a safer and reliable structure design for various applications in the future.

The failure behavior of green composites has recently gains a great attention, especially for certain research area that relates with the composition and characteristic of the natural fibers,

which is relatively difficult to control, and thus, need a particular methods and solution to overcome the difficulties. Also, the environmental factors such as the vibrations and the weathering effects may become an important point that causes a catastrophic failure of the bio-composite materials. These factors are more likely to be related with improper analysis of dynamic loading frequency or inappropriate fiber composition and its compounding behavior. Therefore, the fatigue test - a method for determining the behavior of materials under fluctuating loads - revealed a significant indication on the durability of materials, which is needed to estimate the life span of the material used. The fatigue process of a material is thought to begin at an internal or surface flaw, and the failure effect accumulates after several repetitive loads actions that may caused stress concentration at a point of cumulated damage, that is called as an initial crack point. Then, it generates a shear flow along the slip planes that resembles a crack, and propagates along the weak regions before caused a catastrophic failure. The fatigue study on new materials has become a must in order to design a strong and safety structure with high durability characteristic. A study by Shao Xiong et al. [16] on the properties of flax-epoxy layered composites under fatigue loading underlined the importance of interfacial adhesion between the natural based fillers and hydrophobic resin for the enhancement of the performance of the composites material. Larger number of fiber pulls out and fiber prints indicate the poor adhesion between the flax fibers and epoxy matrix. The interfacial adhesion of green composites had been studied literally; since the combination of these two constituents without the use of an appropriate compitibilizer or coupling agents is commonly lessen the properties of the materials [17]. Indeed, the enlargement of natural based fibers as a potential reinforcement agent in composite material leads to interesting findings, nevertheless, undiscovered factors and behaviors that result in the failure, which are essential to be predicted and analyzed.

1.2 Objectives and outlines

This study aim to understand the fatigue failure mechanism of particulates filled polymer based composite materials and to clarify the fatigue fracture behavior from the fracture surface observation. For these purposes, two types of composite materials; nanoclay nanocomposites and wood-polymer composites (WPCs) were fabricated and tested. The tensile and fatigue tests were carried out for each type specimen - significant means to clarify the reliability of the materials and to understand the failure mechanism. As for the matrices, epoxy and polypropylene (PP) were used as a binder constituent for nanoclay nanocomposites and WPCs, respectively. The compounding of wood fibers and nanoclay fillers into the polymer matrix brings a structural change that caused by the presence of the micro-structure of the fillers itself or as a result from the clustering of the fillers that is incompatible with the polymer. Here, the distribution of the fillers and the compatibility of natural-based fillers with the hydrophobic polymer matrix were taken as the major subject in this study, i.e. by clarifying the relation between the mechanical properties with these factors, it is expected to fulfill the aims of this study.

In Chapter II, the neat epoxy matrix and nanoclay-epoxy (NE-) composites specimens were prepared with different nanoclay amount to investigate the influence of the nano-size fillers amount to the tensile and fatigue properties. The distribution of nanoclay particles was discussed and evaluated through an analysis conducted at the fatigue fracture surface and at the arbitrary cross-sectional area. It is assumed that the cross-sectional area contains a moderate distribution level that result in the lower stress concentration at as compared with at the fracture surface. The electron probe microanalyzer (EPMA) machine was used to conduct an elemental study on both fracture and cross-sectional surface, and a qualitative analysis was performed from the observation images results. From this chapter, the distribution states of nanoclay particles, i.e. the

agglomeration and clustering state, play an important part in determining the failure factors of this material despite lessen the properties of NE composite materials.

In Chapter III, different coupling agent MAPP amount of WPCs specimens was fabricated in order to investigate the effect of coupling agent on fatigue properties of WPCs. The tensile and fatigue test were carried out for each type of specimen. The obtained mechanical properties were discussed regarding to the different effects of coupling agent amount in the composites that expected to improve interfacial adhesion between wood fibers and PP matrix. The cross-sectional area and the fracture surface were characterized by the SEM and 3D laser microscope, respectively.

In Chapter IV, WPCs specimens with different weight fraction of wood fibers were prepared and the tensile and fatigue tests were carried out for each type specimen. The influence of wood fibers on fatigue properties was clarified and the fatigue fracture behavior was characterized from the image analysis. Moreover, further discussion on the fracture damage mechanism of WPCs will be carried out in this chapter.

Finally, Chapter V summarizes all conclusions obtained from the present studies.

Chapter II Electron Probe-Microanalyzer Evaluation of Fatigue Fracture Surface of Nanoclay–Epoxy Composite Materials

2.1 Introduction

Among the wide possibilities presented by various materials, polymer-based nanocomposites have been used in many applications, particularly in the automotive and packaging industries, because of their rigidity, light weight, and high endurance properties. These materials are anticipated for wider use for other applications. Meanwhile, the incorporation of nano-size fillers such as clay particles into polymer matrix materials of fiber reinforced plastic (FRP) composites has been studied [9, 18]. This study assesses the importance of toughening the matrix material for additional applications of composite materials. To date, many studies have examined the preparation, testing, modeling, and analyses of nanoclay-filled polymer-based composites [19].

Nanoclay is known as an ideal nano filler to improve virgin polymer because of its high aspect ratio, low cost, and ease of availability [20]. Nanoclays are classified into three types based on the condensation ratio of silica to an alumina sheet, such as two-sheet minerals (dimorphic), three-sheet minerals (trimorphic), and four-sheet minerals (tetramorphic) [20]. This filler has 1 nm thickness with up to hundreds of nanometers of length. It consists of several elements such as silicon, aluminum or magnesium, and oxygen.

Montmorillonite is typical nanoclay, which is often used as a reinforcement of nanocomposites. This material is a trimorphic clay, i.e. an alumina sheet is sandwiched by silica sheets, from the smectite family, as shown in Fig. 2.1. The surface of each layer is negatively

charged, which attracts inorganic metal cations such as Fe^{2+}, Ca^{2+}, and Na^{+}, and which forms a positively charged layer that is commonly designated as an interlayer (intergallery) between the clay layers. An organic modification occurring with an exchange of inorganic cations with the organic modifiers, results in an expansion of the interlayer space, which allows the polymer to permeate easily into the galleries, thereby forming intercalated and exfoliated clays within the polymer-based matrix. However, nanoclay platelets are likely to be stacked together to form a clustered phase or combined as agglomerate. They might be unable to function completely as a nano-order reinforcing agent. Poor dispersion methods and the usage of non-modified clay particles or low viscous polymer can contribute to this phenomenon. In most cases, poor dispersion of clay particles during preparation often causes nanoclay agglomeration, and induces a decrease in the mechanical properties of the material.

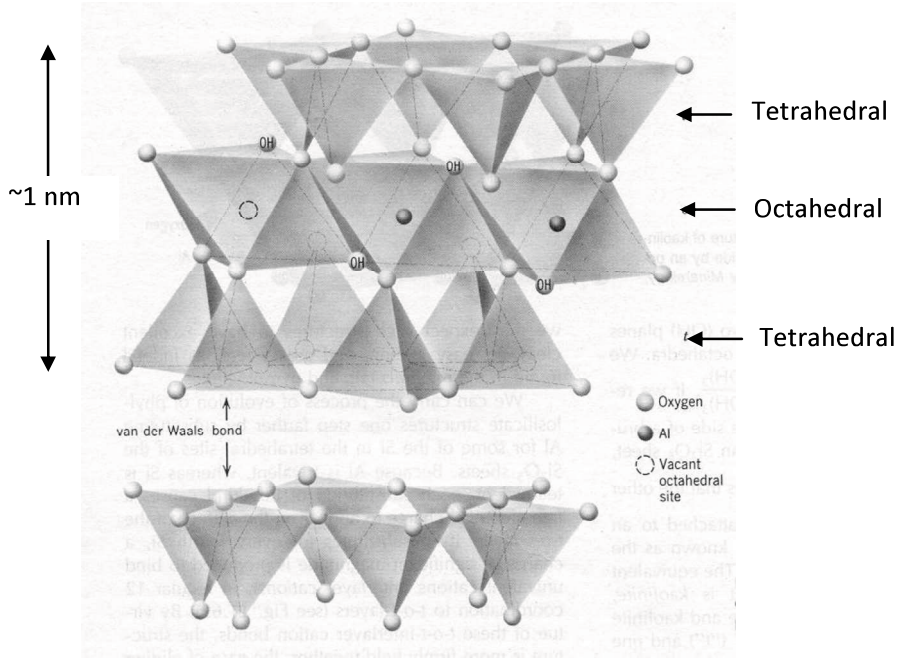

Fig. 2.1 Schematic of chemical structure of montmorillonite mineral.

To realize the importance of morphological analysis of nanoclay cluster or agglomerates, an electron probe micro-analyzer (EPMA) was used in this study. Indeed, this approach is important to ascertain the relation between the microstructure at the fracture surface and mechanical properties. Fatigue failure commonly originates from a local point within the material, at which high stress concentration occurs, resulting in crack initiation. Consequently, this study is of great importance in elucidating how the crack initiation is related with the morphology of the nanoclay cluster or agglomerates in the polymer matrix because the fatigue life of materials often depends on the number of cycles causing the crack initiation.

In this chapter, a study was conducted to introduce quantitative analysis of nanoclay agglomerates for use with observation of fatigue-fractured nanoclay-filled epoxy resin matrix composites, and to clarify nanoclay agglomerates' size and dispersion states. For this purpose, different amounts of nanoclays were incorporated into the resin through the conventional mechanical and ultrasonic processes. Analyses were conducted using EPMA at arbitrary and crack initiation areas on the fatigue-fractured surface. Finally, we examined the affinity between the results obtained from quantitative analysis and fatigue tests.

2.2 Experimental methods

2.2.1 Materials

In this study, bisphenol-F type epoxy resin (EP-4901, Density: 1.19 Mg/m^3) was used as a matrix material, and polyetheramine hardener (Jeffamine T-403, Density: 0.978 Mg/m^3; Huntsman Co., Ltd.) was used as a curing agent as shown in Fig. 2.2. Both EP-4901 and Jeffamine T-403 were mixed in the weight ratio of 100:46 to produce a thermosets resin. Regarding reinforcement, nanoclay (Nanomer®I.28E, Bulk density: 0.25-0.30 Mg/m^3; Nanocor Inc.) was used as shown in Fig. 2.3. As described in earlier reports, clay particles can be dispersed properly throughout the polymer matrix despite small weight percent values [9, 18, 21–23]. Consequently, it is expected that the clay particles can create much higher surface area for polymer/filler interaction than conventional micro-order clays can.

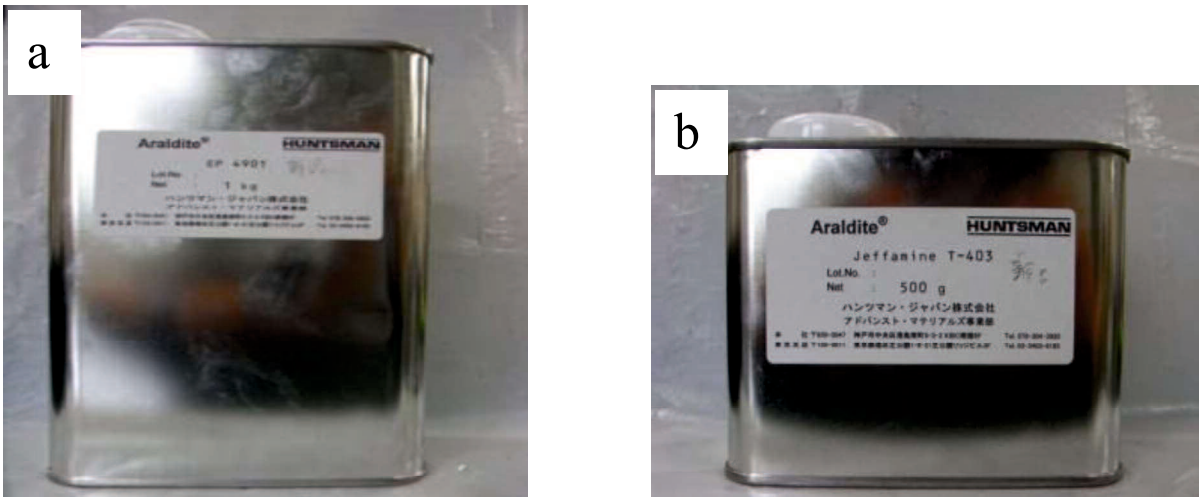

Fig. 2.2 Overview of (a) bisphenol-F type epoxy resin and (b) polyetheramine hardener.

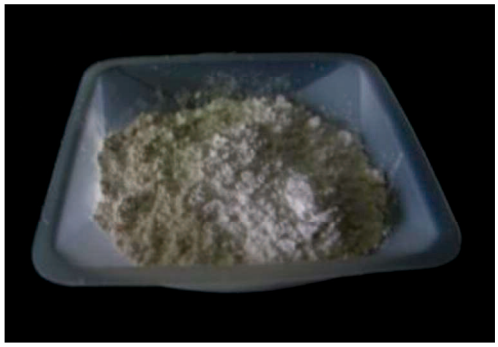

Fig. 2.3 Overview of nanoclay powder, Nanomer®I.28E.

2.2.2 Specimen fabrication

First, 1 phr, 3 phr, or 5 phr of nanoclay amounts were measured. They were mixed with EP-4901 epoxy resin in a beaker with a mechanical stirring device (PM-201; As-One Corp.) at 2500 rpm for about 3 min. Then, the mixture was mixed further using an ultrasonic homogenizer device (Branson Sonifier 450; CSC Co.) for another 10 min. An overview of the mechanical stirring device and the ultrasonic homogenizer are shown in Fig. 2.4. During the sonication process, the beaker was placed in cold water to avoid increasing the solution's temperature [9]. The solution's temperature was measured using a thermometer every one minute. Subsequently, the Jeffamine T-403 hardener was added to the solution and was stirred manually for about three more minutes at room temperature.

Then, nanoclay–epoxy resin solution was poured into a metallic mold as shown in Fig. 2.5. A mold lubricant (QZ13; Huntsman Co., Ltd.) was applied beforehand to prevent adhesion to the metallic mold of the epoxy resin. The mold was then placed in a vacuum pump for 10 min to remove air bubbles from the resin. The specimens were cured completely after placing them in a homo-isothermal drier (MOV-112F; Sanyo Co.) for 24 h at 30 °C; then for 6.5 h at 60 °C. The

nanoclay volume fractions of 1 phr, 3 phr, and 5 phr specimens were 0.007, 0.019, and 0.032 respectively. The overview of vacuum pump and the homo-isothermal drier are shown in Fig. 2.6.

The specimen dimensions of tensile and fatigue tests are presented in Fig. 2.7. The thickness and width of each specimen were measured respectively at three points: both ends and the center of the gauge part. These average values were recognized respectively as the specimen thickness and width. Then, the aluminum tabs were attached to both ends of the specimens using an adhesive.

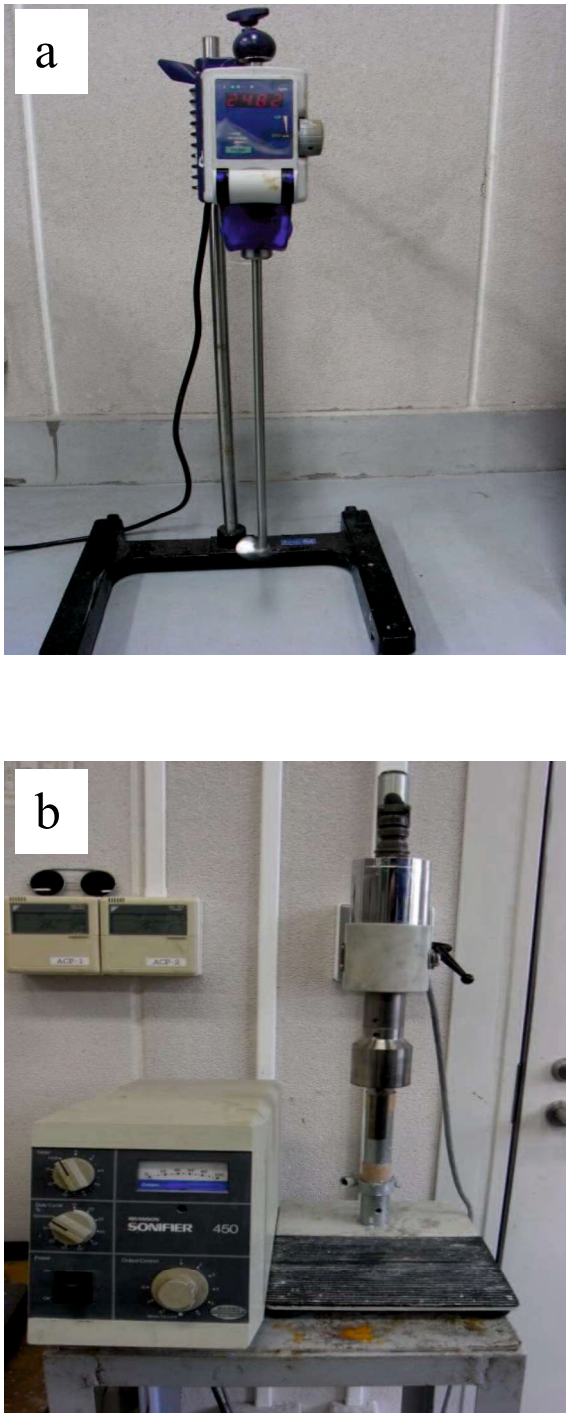

Fig. 2.4 Overview of (a) mechanical stirring device and (b) ultrasonic homogenizer.

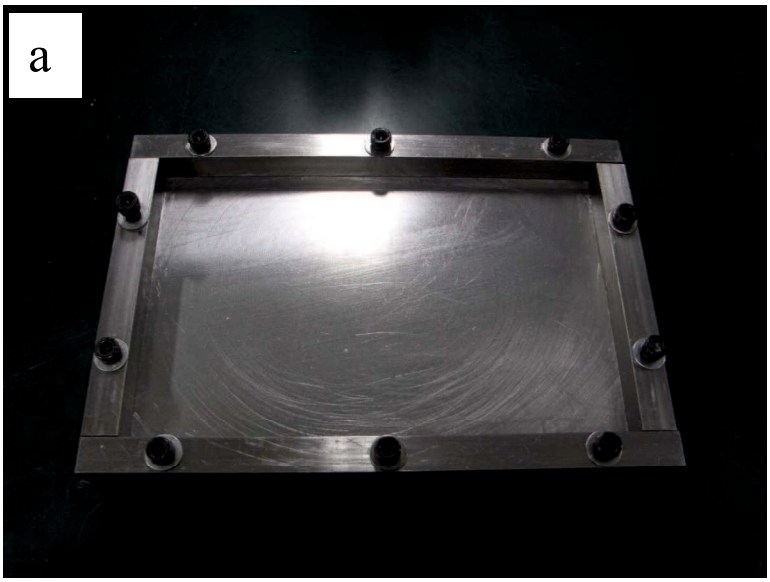

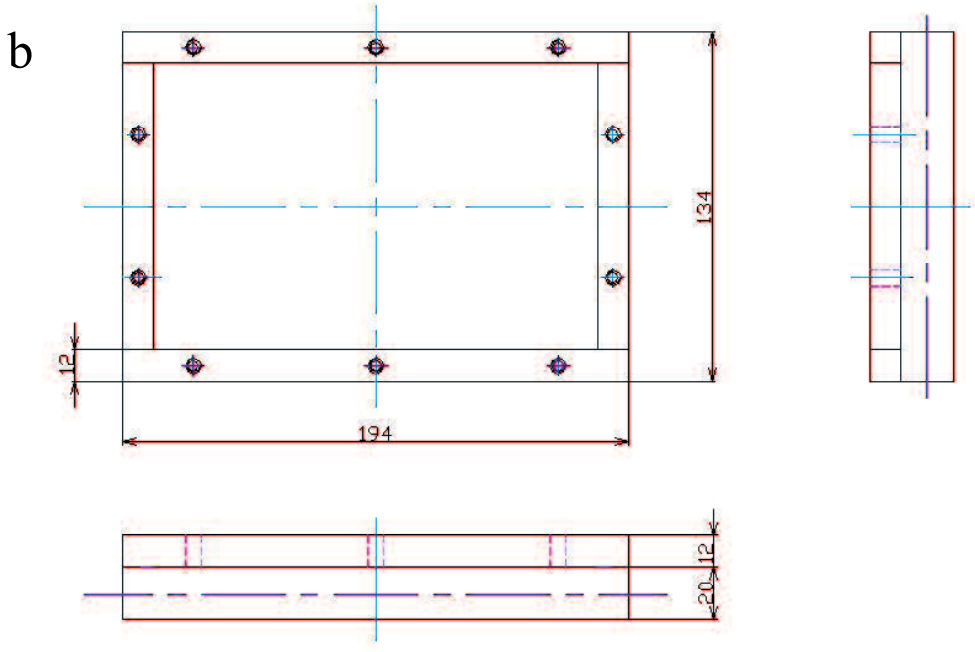

Fig. 2.5 Overview of metallic mold.

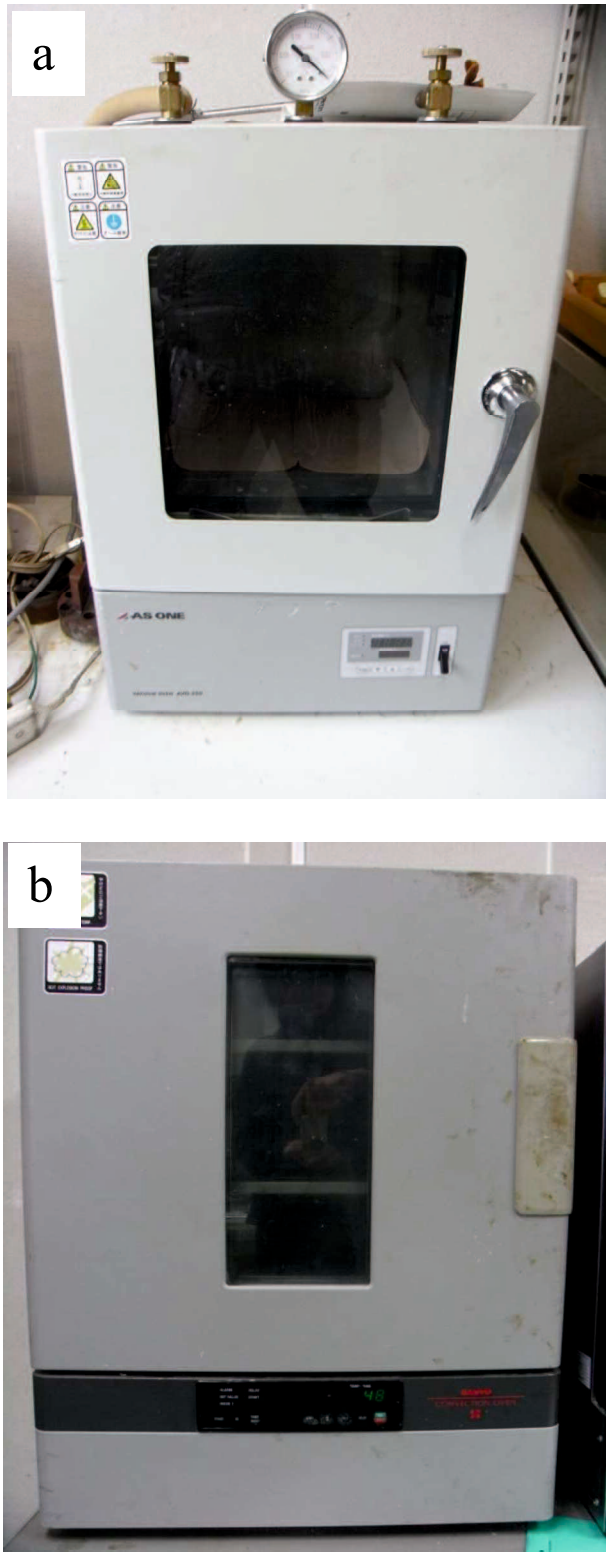

Fig. 2.6 Overview of (a) vacuum pump and (b) the homo-isothermal drier.

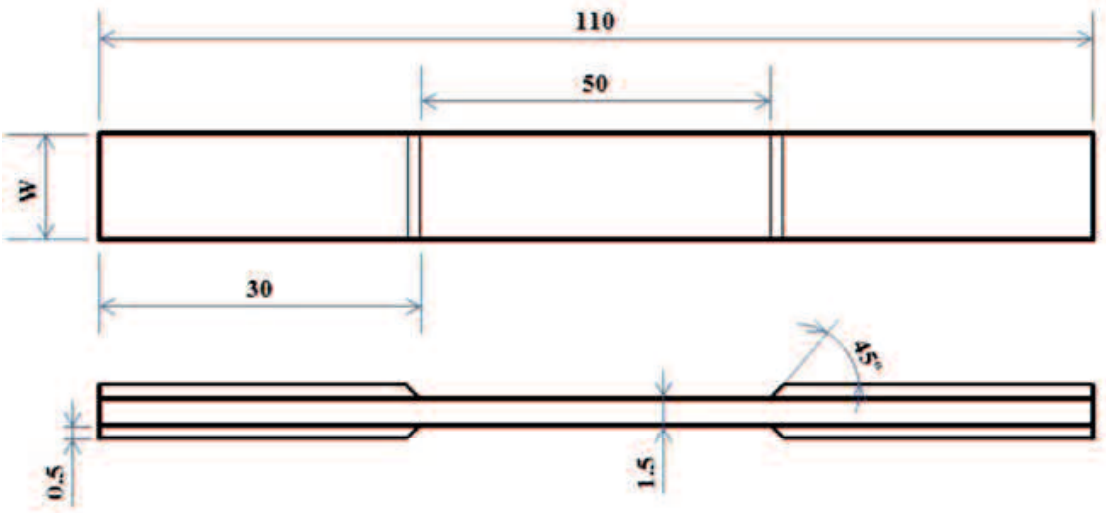

Fig. 2.7 Specimen shapes and dimensions (W=16 mm for tensile specimen; W=10 mm for fatigue specimen).

2.2.3 Tensile and fatigue tests

An Instron-type testing machine (49.03 kN load capacity, Autograph IS5000; Shimadzu Corp.) as shown in Fig. 2.8, was used to determine the tensile properties of each type of specimen. A strain amplifier (DPM-700B; Kyowa Electronic Instruments Co. Ltd.) and a strain gauge (KGF-5-120-C1-11L1M2R; Kyowa Electronic Instrument Co. Ltd.) were used for strain measurements during the tensile test. Fig. 2.9 shows the strain amplifier and strain gauge that was used in this study. Tensile tests were conducted at the crosshead speed of 1 mm/min up to fracture at room temperature. The number of cycles to failure of each specimen was measured through a fatigue test using an electric oil pressure servo type material testing machine (9.8 kN load capacity, Servo pulser EHF-FBI-4LA; Shimadzu Corp.) as shown in Fig. 2.10, at room temperature. The fatigue test was conducted at 44%–77% levels of static fracture load obtained in the tensile test, and up to fracture or achieving 10^4 cyclic numbers. The stress ratio used here was 0.1. The frequency was 5 Hz.

Fig. 2.8 Overview of Instron-type testing machine.

a

b

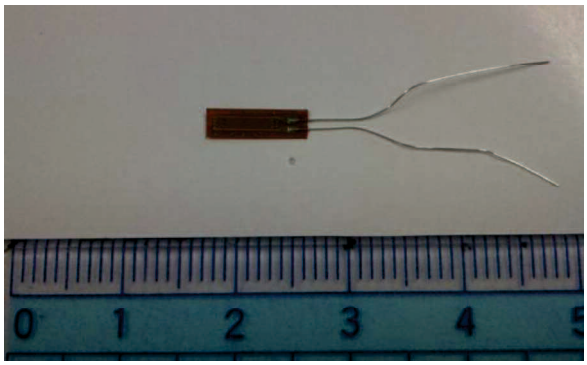

Fig. 2.9 Overview of (a) strain amplifier and (b) strain gauge.

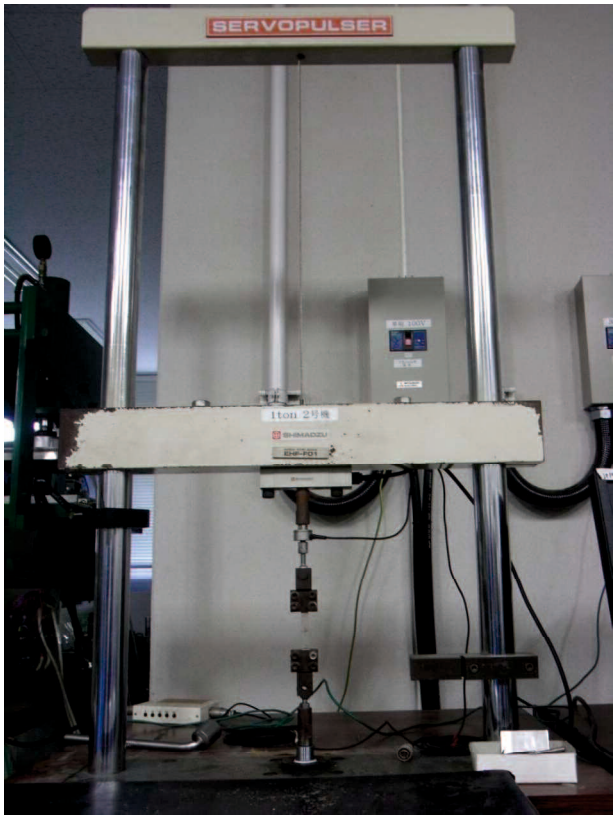

Fig. 2.10 Overview of an electric oil pressure servo type material testing machine.

2.2.4 Elemental observation

To investigate the distribution and size of nanoclay agglomerates, two parts from the fatigue tested specimens, i.e., fracture surface and arbitrary cross-section, were observed through the electron probe micro-analyzer (EPMA-V6; Shimadzu Corp.). Three main elements of nanoclay: silicon (*Si*), aluminum (*Al*), and magnesium (*Mg*), were chosen and analyzed through EPMA at each part of all specimens types. For the fracture surface observation, each of the fractured specimens was cut into approximately 5-mm-long pieces from the fracture surface. For comparison, samples of similar length were cut at arbitrary cross-sections of each type specimen to observe the presence of nanoclay at the cross-sectional surface (Fig. 2.11). Because the resin itself is an insulator, the golden vapor deposition was conducted for each sample using micro-ion

weld slag equipment. After this procedure, those samples were observed for both point and area analyses, as described later. The beam sizes used were 10 μm and 1 μm, respectively, for the point and area analyses. The sample current and voltage used for EPMA were, respectively, 0.1 mA and 15.0 kV.

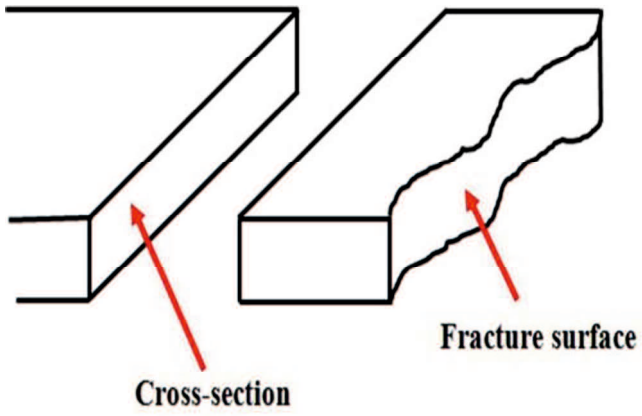

Fig.2.11 Schematic figure of section taken for fracture surface and cross-section sample preparation.

2.3 Experimental results

2.3.1 Tensile and fatigue properties

Average values of tensile strength, fracture strain, Young's modulus, and fracture load are presented in Table 2.1 for neat and nanoclay–epoxy specimens. The average value of the tensile strength of the 1phr specimen is similar to that of the neat specimen. However, 3phr and 5phr specimens decreased respectively to 74% and 67% levels. With conventional physical mixing process, it is predicted that a higher amount of nanoclay brings formation of more agglomerates or agglomerate clustering, which induces premature fracturing. However, the Young's modulus is improved slightly by adding nanoclay in 3 phr and 5 phr specimens. This result presents a similar trend to those reported from other studies [5, 24], which suggests that the existence of clay agglomerates of a certain number and size decreased the strength. However, the high modulus clay particles are expected to improve the polymer stiffness. More detailed predictions related to failure mechanisms are difficult to make merely based on tensile test results.

Table 2.1 Tensile properties of neat and nanoclay–epoxy specimens.

Specimen type	Number of specimens	Tensile strength [MPa]	Fracture Strain [%]	Young's modulus [GPa]	Fracture load [N]
neat	5	60.5	4.19	3.34	892
1phr	5	60.7	3.06	3.33	899
3phr	5	48.0	2.13	3.56	797
5phr	5	45.4	1.42	3.40	645

A fatigue test was conducted based on the fatigue loads, which were determined from the static fracture loads in Table 2.1. The relation between the applied maximum stress and fatigue

life for each specimen is depicted in Fig. 2.12. Here, the experimental data from fatigue tests are shown as a semi-logarithmic graph and are approximated using a regression curve delineated from a double-logarithmic scale. From this figure, results show that the fatigue life of 1phr specimens is slightly shorter than that of neat specimens, although tensile properties of 1phr specimens are comparable to those of neat specimens. The fatigue life is greatly reduced for both 3phr and 5phr specimens, similarly to tensile properties, except for the Young's modulus. This result probably derives from premature fatigue crack initiation in the specimens, which is expected to be related with the amount of clay addition into the epoxy resin.

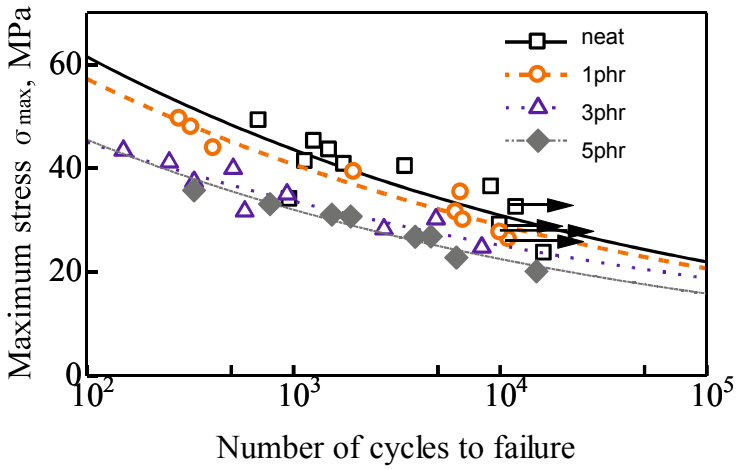

Fig. 2.12 S–N curves of neat and nanoclay–epoxy specimens.

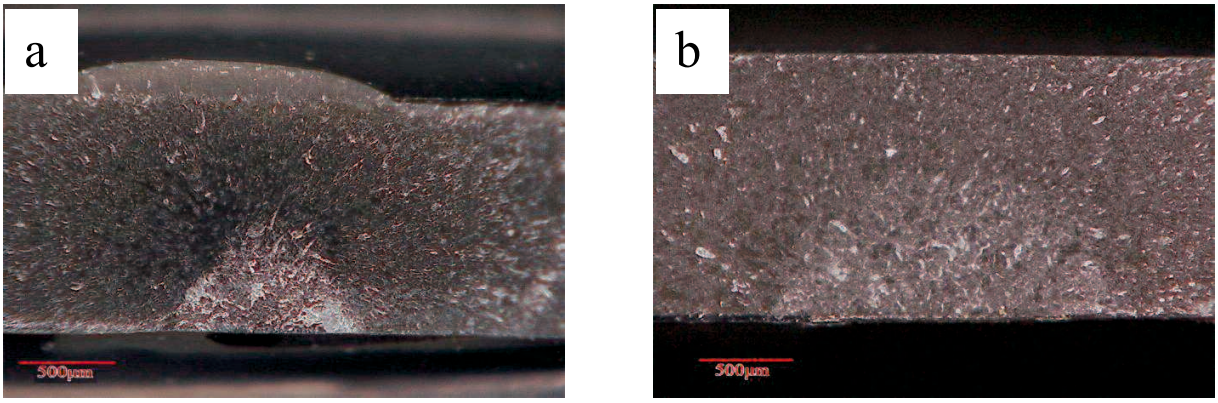

Fig. 2.13 Typical fatigue fracture surface of (a) 1phr and (b) 3phr specimens.

Figures 2.13a and b respectively present optical micrographs of fatigue fracture surfaces at a 50% level of static fracture load for 1phr and 3phr specimens. As the figures show, the fatigue crack initiation and propagation initiate from a point, on the fracture surface of each specimen. The fatigue fracture surface exhibited a clearer morphology related to the fracture process as compared with tensile fracture surface. It can be inferred from the fatigue fracture surface that the crack occurs from a weak point, i.e., a local region where agglomerates or clay cluster exist, as shown later, and propagates across the weak region at a cross section before it is fractured.

2.3.2 EPMA observation

Point analysis was first done for 1phr, 3phr, and 5phr samples, in which both the fatigue fracture surface and arbitrary cross-section were divided into 10 sections in a zigzag pattern along the width direction. Furthermore, the beam was applied at the center of each section. The results are presented in Fig. 2.14, in which the point analysis of *Si* is shown because *Si* revealed the agglomerates with a sharp boundary image compared with the other detected elements, as shown later. It can be readily observed that, although the *Si* intensity increases concomitantly

with increasing clay content, the peak intensity on the fracture surface is greater for any clay content than that of the cross section. Furthermore, this difference was apparent in all fatigue load conditions. The fracture surface tends to include more nanoclays than arbitrary cross-sections, irrespective of the crack initiation position.

Next, area analysis was conducted at a limited area of 500 μm × 500 μm, which was done for each condition not only at the areas including peak intensity points on the fatigue fracture surface and arbitrary cross-section, but also at the fatigue crack initiation area. Figures 2.15a, b and c respectively show representative image results of *Si*, *Mg*, and *Al* elemental analyses at arbitrary cross-sections of the 5phr specimen. Results confirmed that all detected elements are located at almost the same position in any figure, as indicated by the arrow. Therefore, we recognize these detected elemental distributions as the morphology and position of clay agglomerates or clusters. In comparison with the figures, *Si* elements are displayed more clearly with less noise than others. Hereinafter, we use it as a typical clay distribution map.

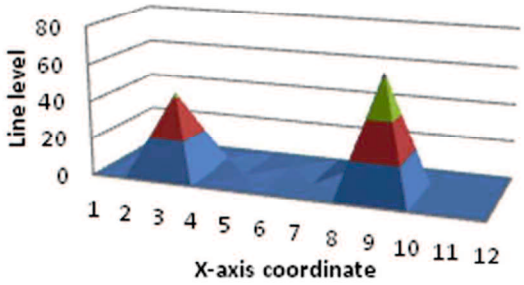

a

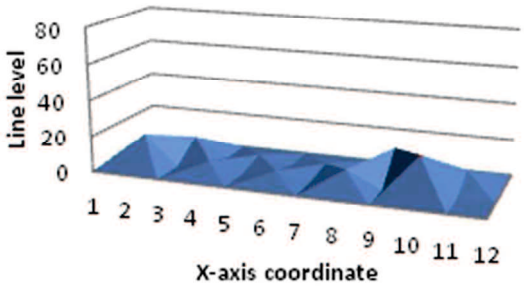

d

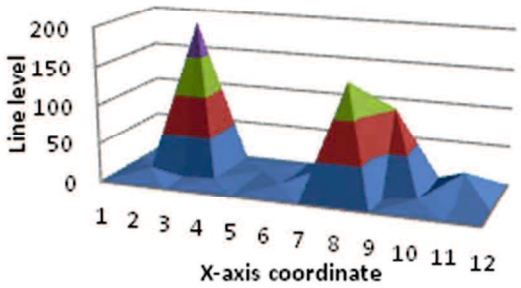

b

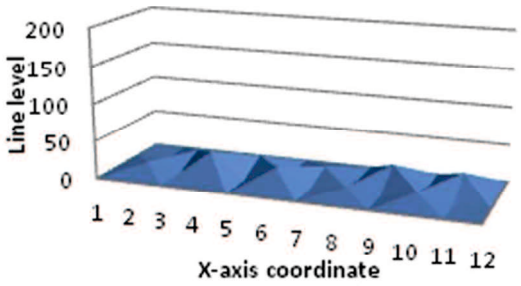

e

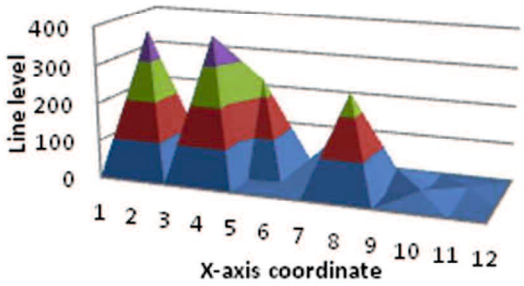

c

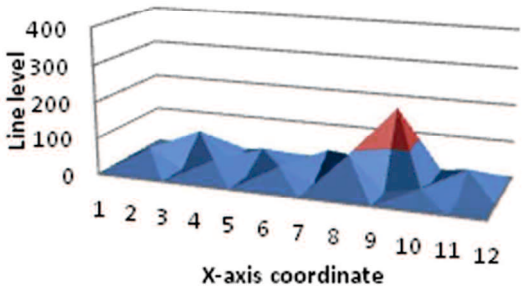

f

Fig. 2.14 Point analysis of *Si* element of 1phr (60% level of static fracture load), 3phr (60% level of static fracture load), and 5phr (66% level of static fracture load) fatigue-tested specimens at both fracture surface (a)–(c) and arbitrary cross-section (d)–(f).

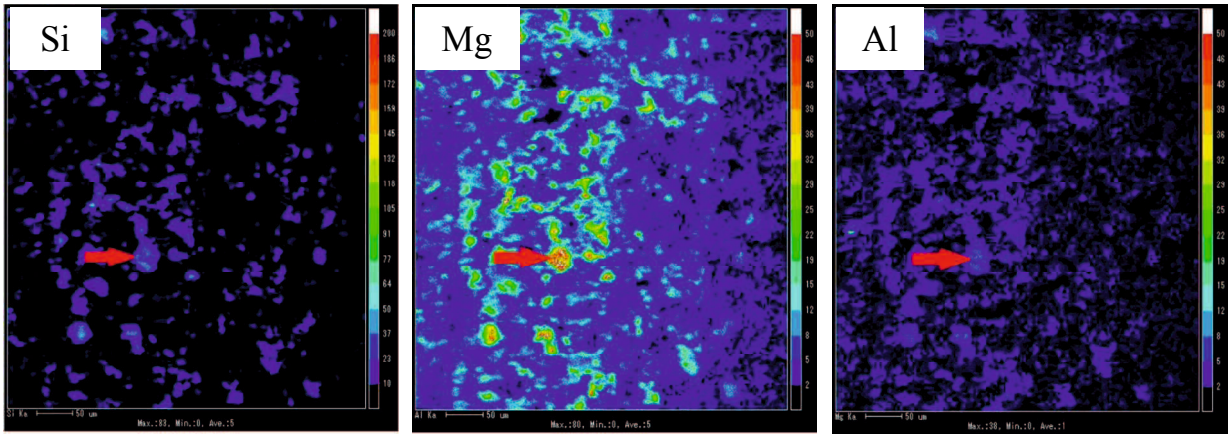

a b c

Fig. 2.15 Representative EPMA image results of (a) *Si*, (b) *Al*, and (c) *Mg* elemental analyses at arbitrary cross-sections of a 5phr specimen.

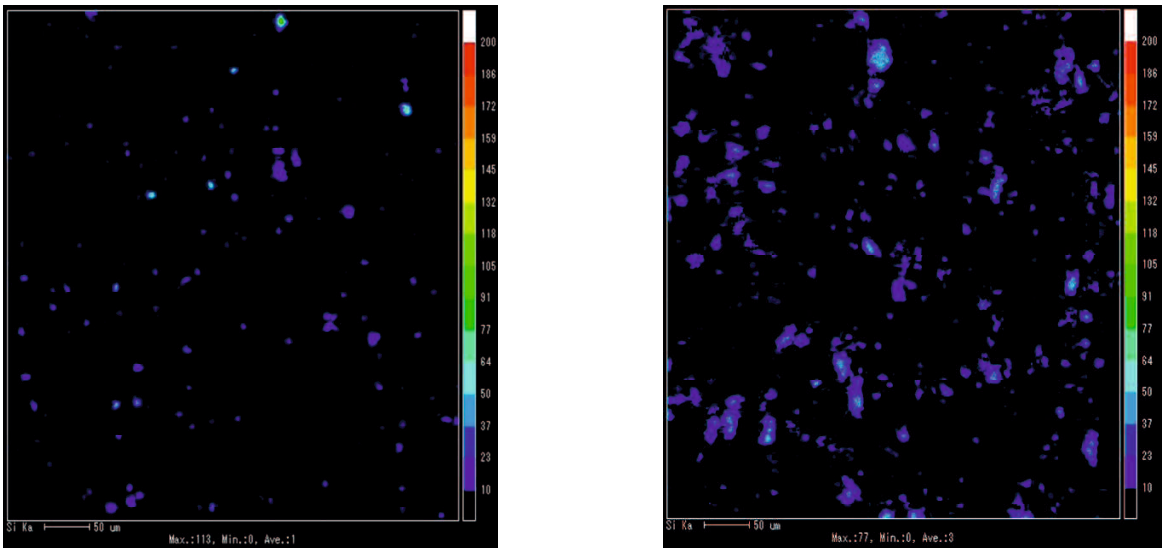

a b

Fig. 2.16 EPMA image result of *Si* at an arbitrary cross-section of (a) 1phr and (b) 3phr specimens.

Figures 2.16a and b respectively show representative image results of *Si* elemental analysis at the arbitrary cross-sections of 1phr and 3phr specimens. From these images and Fig. 2.15a, it is understood that clay particles tend to be clustered or formed into microscale agglomerates in the epoxy resin, but, as for the 1phr specimen, clay particles are well dispersed within a similar small size. The agglomerate area size of 1phr and 3phr specimens is 32 μm^2 on average, whereas that of the 5phr specimen is approximately 44 μm^2, as shown in Table 2.2, as estimated using image analysis software. It is also confirmed that all parameters such as the number, area ratio, and average and maximum sizes of agglomerates, increase with increasing nanoclay content.

Table 2.2 Average values of EPMA area analysis results at arbitrary cross section of 1phr, 3phr, and 5phr specimens.

Specimen type	Number of agglomerates	Area ratio [%]	Average size of agglomerate [μm^2]	Maximum size of agglomerate [μm^2]
1phr-C	171	2.20	32.1 (6.39)	616 (28.0)
3phr-C	534	6.28	32.5 (6.43)	1385 (42.0)
5phr-C	860	12.31	43.7 (7.46)	3650 (68.2)

(∗): estimated diameter value in case agglomerates are assumed as a circle.

Fig. 2.17 shows EPMA image results for 1phr, 3phr, and 5phr specimens: (a) fatigue fracture peak intensity area and (b) fatigue crack initiation area. F_{pi} and F_{ci} attached to the sample's name are the abbreviations of the fatigue fracture peak intensity and fatigue crack initiation, respectively. From Fig. 2.17, F_{pi} and F_{ci} areas contain more agglomerates than the peak intensity areas at arbitrary cross-section portrayed in Fig. 2.16, similarly to the result of point analysis in Fig. 2.14. Comparison between F_{pi} and F_{ci} areas shows that the latter contains slightly

more agglomerates. According to the image analysis results in Table 2.3, as the nanoclay content increases, the number of agglomerates, area ratio and maximum agglomerate size increase, although the average size of agglomerates does not change so much. This is because small and normal size agglomerates are predominantly many, independent of nanoclay content. Consequently, the size of agglomerates is distributed more widely with a statistical variation with increase in nanoclay content, but resembles in average each other.

Table 2.3 Average values of EPMA area analysis results for F_{pi} and F_{ci} of 1phr, 3phr, and 5phr specimens.

Specimen type and area	**Number of agglomerates**	**Area ratio [%]**	**Average size of agglomerate [μm^2]**	**Maximum size of agglomerate [μm^2]**
1phr-F_{pi}	160	2.00	38.0 (6.96)	706 (29.98)
1phr-F_{ci}	205	2.20	36.4 (6.81)	920 (34.23)
3phr-F_{pi}	522	13.0	66.0 (9.17)	1607$^{\#}$ (45.23)
3phr-F_{ci}	596	12.9	75.8 (9.82)	2560$^{\#}$ (57.09)
5phr-F_{pi}	725	14.0	60.0 (8.74)	2563 (57.13)
5phr-F_{ci}	764	17.9	65.7 (9.15)	2121 (51.97)

(∗): estimated diameter value in case agglomerates are assumed as a circle.

$^{\#}$: 50% level of fracture load specimens data are excluded.

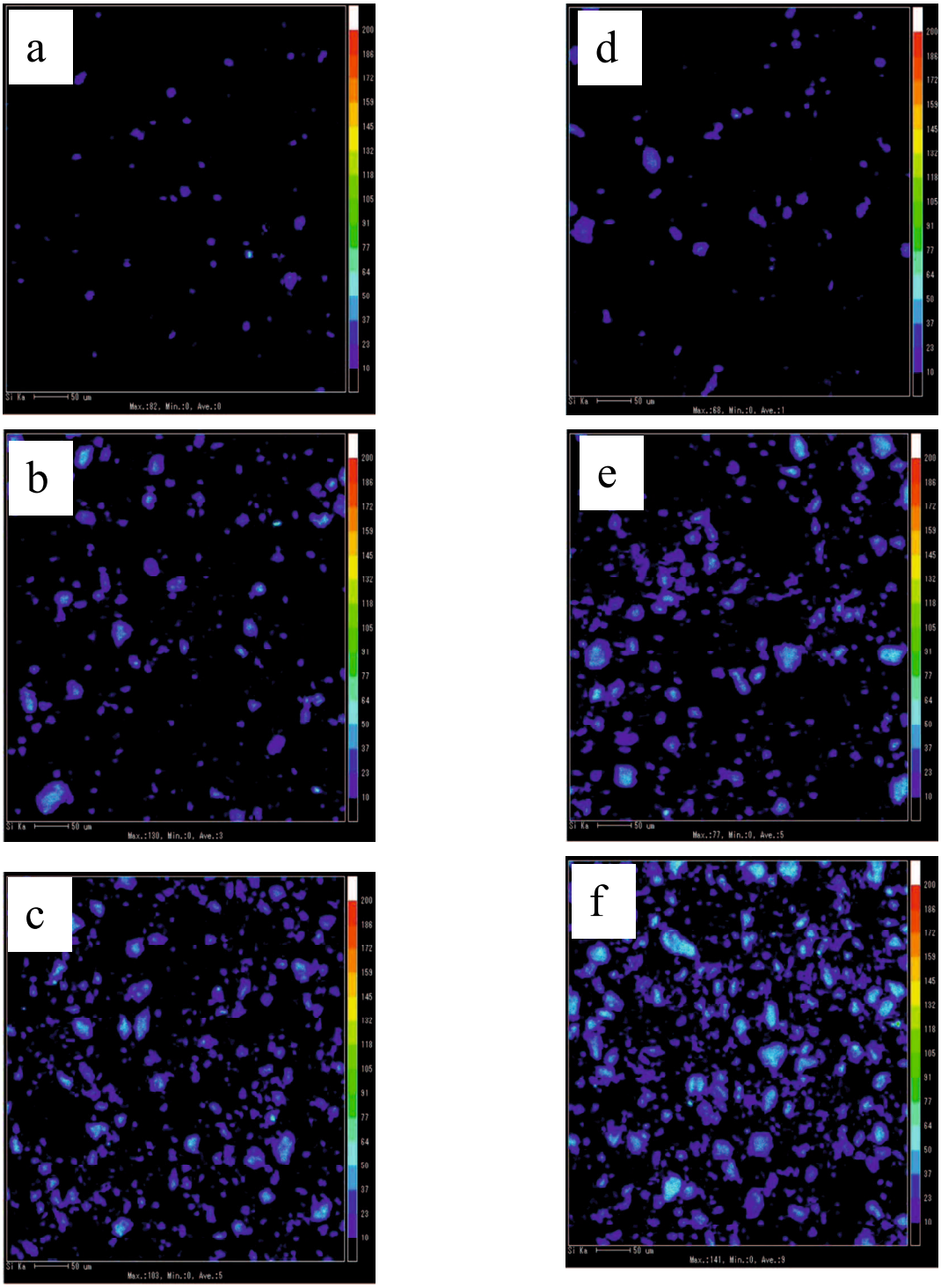

Fig. 2.17 EPMA image result of 1phr, 3phr, and 5phr specimens at F_{pi} (a)–(c) and F_{ci} (d)–(f) surfaces.

In Table 2.3, it is noteworthy that the maximum agglomerate size of F_{ci} is larger than F_{pi} for any sample type, and in 1phr and 5phr specimens, the respective numbers of agglomerates of F_{ci} and F_{pi} are almost identical. Consequently, it is considered that the number of large agglomerates and the maximum size are related to the cause of less fatigue life of the specimens. In addition, Tables 2.2 and 2.3 show that, especially as might be readily apparent from the comparison between the results of 1phr specimen, even if most of the nanoclay particles are well dispersed or exfoliated in the resin, large locally existing agglomerates have a risk of causing premature fatigue crack initiation.

2.4 Discussion

2.4.1 Agglomerate evaluation by image analysis

In most studies, the failures of nanocomposites are commonly reported as related with the existence of clay agglomerates and the consequent effects of surrounding stress concentration [23]. However, a comparison of Figs. 2.16 and 2.17 demonstrates clearly that the characteristics of the failure of a material are not only those related to the presence of agglomerates. Other factors are expected to involved, such as the size and number of large scale agglomerates, as described above, which are expected to affect the level of stress concentration brought from their mutual interaction. In addition, although it is impossible or at least very difficult to observe the sub-micrometer order aspect, such as the exfoliation state of clay particles, because of some limitations, EPMA elemental analysis can be recommended as a useful method to interpret the dispersion order of clay agglomerates microscopically on the surfaces.

This study revealed a hint of the fatigue fracture mechanism from the image analysis results of 1phr, 3phr, and 5phr specimens. In Table 2.4, the image analysis result is arranged for every applied fatigue load at both F_{pi} and F_{ci} areas. Results show that at the crack initiation area, the overall values of the total number, area ratio and average size of agglomerates do not necessarily indicate more than that of the values at the peak intensity area. In other words, these parameters do not give a strong indicator to be associated with the failure of the materials. However, the crack initiation area tends to represent a larger maximum size of agglomerates than the peak intensity area. We therefore consider that the maximum size parameter more strongly influences the premature crack initiation and fatigue life.

To investigate the relation between the maximum size of agglomerates and the fatigue lives, the following method was conducted: First, a deviation was found between the fatigue life regression line and each number of cycles to failure was calculated as portrayed in the S–N diagram (Fig. 2.12). Table 2.5 shows the result of the calculated deviations, which are given in log scale. Positive values of the deviation number denote more numerous cycles than the regression line; negative values denote less numerous cycles. Next, the correlation coefficients between the maximum size of agglomerates at the fatigue crack initiation area and the deviation values were calculated. The calculated values are presented in Table 2.6 for 1phr, 3phr, and 5phr specimens.

Table 2.4 EPMA area analysis results for F_{pi} and F_{ci} of 1phr, 3phr, and 5phr fatigue specimens.

Applied fatigue load		1phr				3phr				5phr			
		Number of agg.	Area ratio (%)	Ave. size of agg. [μm^2]	Max. size of agg. [μm^2]	Number of agg.	Area ratio (%)	Ave. size of agg. [μm^2]	Max. size of agg. [μm^2]	Number of agg.	Area ratio (%)	Ave. size of agg. [μm^2]	Max. size of agg. [μm^2]
77%	F_{pi}	250	3.59	35.92 (6.76)	1114 (37.66)	527	10.5	49.82 (7.96)	1882 (48.95)	866	13.08	37.77 (6.94)	1522 (44.02)
	F_{ci}	81	1.33	41.16 (7.24)	280 (18.88)	509	9.41	46.21 (7.67)	2151 (52.33)	-	-	-	-
72%	F_{pi}	178	2.41	33.84 (6.56)	516 (25.63)	155	7.28	117.4 (12.2)	1042 (36.42)	803	12.74	39.66 (7.11)	1794 (47.79)
	F_{ci}	152	2.36	38.85 (7.03)	878 (33.44)	806	3.31	10.28 (3.62)	1381 (41.93)	817	16.72	51.15 (8.07)	2023 (50.75)
66%	F_{pi}	163	3.95	60.56 (8.78)	1032 (36.25)	557	14.07	63.16 (8.97)	2155 (52.38)	910	19.44	53.41 (8.25)	2342 (54.61)
	F_{ci}	125	2.65	52.98 (8.21)	2495 (56.36)	613	18.58	75.78 (9.82)	4601 (76.54)	751	14.31	47.63 (7.79)	1480 (43.41)
65%	F_{pi}	-	-	-	-	480	6.86	35.74 (6.75)	1377 (41.87)	873	14.28	40.89 (7.22)	1238 (39.70)
	F_{ci}	-	-	-	-	796	18.92	59.44 (8.70)	3789 (69.46)	891	17.14	48.09 (7.83)	1622 (45.44)
60%	F_{pi}	183	2.02	27.54 (5.92)	403 (22.65)	616	11.84	48.04 (7.82)	1892 (49.08)	971	14.37	36.69 (6.84)	1846 (48.48)
	F_{ci}	137	0.40	7.26 (3.04)	167 (14.58)	724	4.67	16.12 (4.53)	1717 (46.76)	942	19.35	51.36 (8.09)	2103 (51.75)
55%	F_{pi}	93	0.78	21.10 (5.18)	257 (18.08)	644	16.38	63.57 (9.00)	1779 (47.59)	288	10.82	93.89 (10.9)	942 (34.63)
	F_{ci}	131	2.38	45.47 (7.61)	718 (30.24)	593	8.01	33.75 (6.56)	2756 (59.23)	418	21.79	130.3 (12.9)	3379 (65.59)
50%	F_{pi}	120	2.43	50.61 (8.03)	1114 (37.66)	512	22.77	111.2 (11.9)	26870 (185.0)	357	16.39	114.8 (12.1)	8254 (102.5)
	F_{ci}	213	5.63	66.03 (9.17)	1648 (45.81)	228	28.91	307.6 (19.8)	26185 (182.6)	-	-	-	-
44%	F_{pi}	136	1.91	35.19 (6.69)	504 (25.33)	681	11.51	42.25 (7.33)	1120 (37.76)	-	-	-	-
	F_{ci}	594	0.64	2.68 (1.85)	249 (17.81)	502	11.48	57.18 (8.53)	1528 (44.11)	-	-	-	-

(*): estimated diameter value in case agglomerates are assumed as a circle.

Table 2.5 Deviations in log scales of fatigue life for respective specimens.

Specimens	P_{max}							
	77%	72%	66%	65%	60%	55%	50%	44%
1phr	0.079	0.011	-0.199	-	0.118	0.325	0.000	-0.083
3phr	0.124	0.295	0.113	0.053	-0.491	0.280	-0.169	-0.055
5phr	-0.111	-0.017	0.129	0.073	0.122	0.039	-0.176	-

Table 2.6 Correlation coefficient of maximum size of agglomerates and the nearest neighbor function $G(R)$.

	1phr	3phr	5phr
Maximum size of agglomerates	-0.54	-0.26	-0.39
Nearest neighbour function *G(R)*	-0.56	-0.21	-0.73

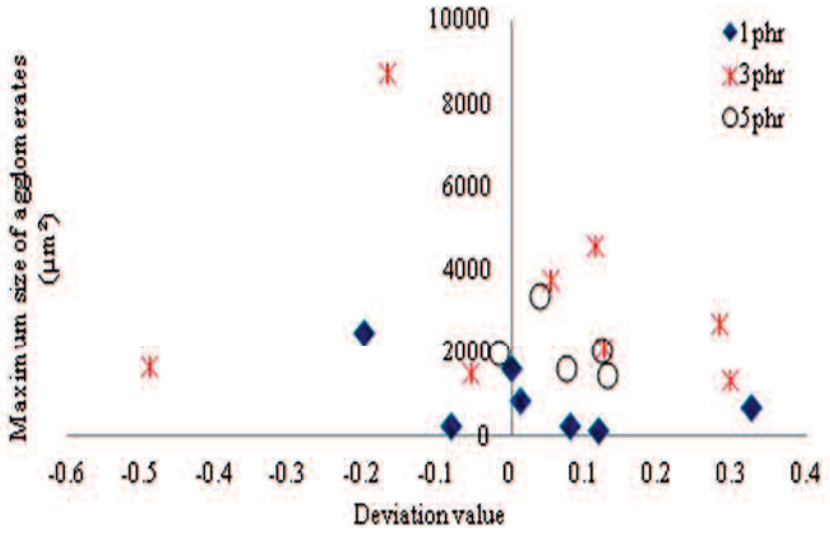

Fig. 2.18 Relation between maximum size of agglomerates and deviation of fatigue life curves.

Figure 2.18 shows a correlation graph for specimens of each type. We consider that a negative correlation coefficient of more than 0.4 in absolute value [25] implies that the maximum size is a reasonable parameter to some degree to express the variation in fatigue life. Although the negative correlation coefficient was estimated from specimens of each type, 3phr and 5phr specimens are not satisfied with the condition of more than 0.4. However, the 1phr specimen is satisfied with the condition, so that this suffers the influence of large scale agglomerates to some degree, resulting in the low fatigue life. It is estimated for a 1phr specimen that the premature cracks, which can be denoted as microcracks as well, are easily formed between the nanoclay platelets that are weakly bonded, where these probably coexist with a small amount of epoxy and voids. At this point, Wang et al. [26] had discussed details on the micro deformation and fracture mechanism of epoxy nanocomposites related to the presence of agglomerates within the exfoliated clay. They pointed out that the microcracks are initiated in between the clay layers rather than at the epoxy–clay interface, i.e. the clay interlayer is weaker than epoxy–clay interfacial bonding, resulting in interlaminar debonding (microcrack). Here, a

CT scan was employed to a small part of nanoclay nanocomposites in order to get a clear visual on the distribution of nanoclay at each micron-layer of the specimens, i.e., the scanning images was taken from the top surface of the specimen to the bottom for each layer. Fig. 2.19 shows one of the images from the CT scan image analysis result. From this figure, it is point out that the microcracks are likely emerged in the middle of nanoclay agglomerates. Additionally, we consider that large-scale agglomerates, such as the maximum size described above, often include micro-voids because the resin does not infiltrate until the center of the agglomerates. One might say that the voids can readily produce a crack during fatigue loading.

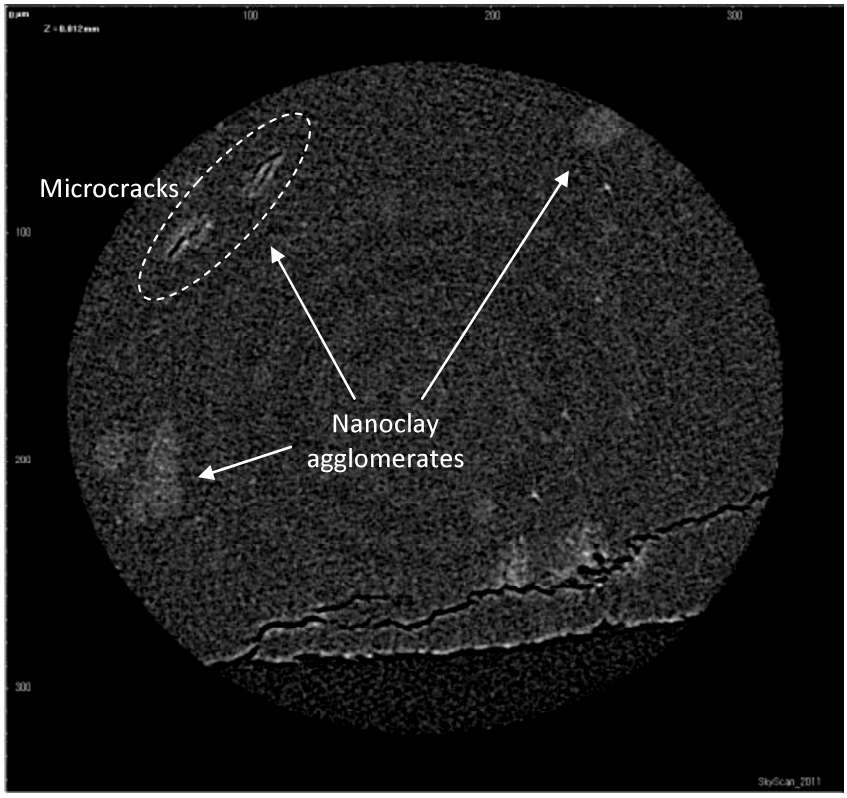

Fig. 2.19 CT scan images on a small part of tensile specimens indicate the microcracks (circled by white dotted line) that emerged in the middle of nanoclay agglomerates.

Consequently, it is estimated that, as the stress concentration is increased gradually, the microcracks formed within the agglomerates also increase, and mutually coalesce, including cracks brought from micro-voids, and develop to a fatigue crack initiation that finally engenders fatigue failure of the composite materials. However, this mechanism might be valid only for 1phr specimens, but does not necessarily interpret 3phr and 5phr specimens because each was not evaluated as the satisfied value, i.e. more than 0.4 of the correlation coefficient. The insufficient number of observed specimens might also be one reason. Therefore, we extend the discussion from the viewpoint of spatial analysis in the next section.

2.4.2 Evaluation using the nearest neighbor functions

We consider in this section that microcracks are linked together not only in agglomerate, but also between neighbors. In other words, the fatigue crack initiation might be related with interaction between agglomerates if the agglomerates are close together. Consequently, to investigate the correlation between the dispersion state of agglomerates and the fatigue life deviations, a quantitative evaluation was conducted.

In general, the ideal particle dispersion is regarded as a random distribution. However, the particles or agglomerates are often distributed with localization. This phenomenon is called ‘clustering’. Clustering is evaluated using several methods, such as the nearest neighbor function and *L*-function. In this study we use the nearest neighbor function $G(R)$, a relatively simple analysis. $G(R)$ function can be determined by the average distance of the nearest nanoclay agglomerates for the n count number of nanoclay agglomerates.

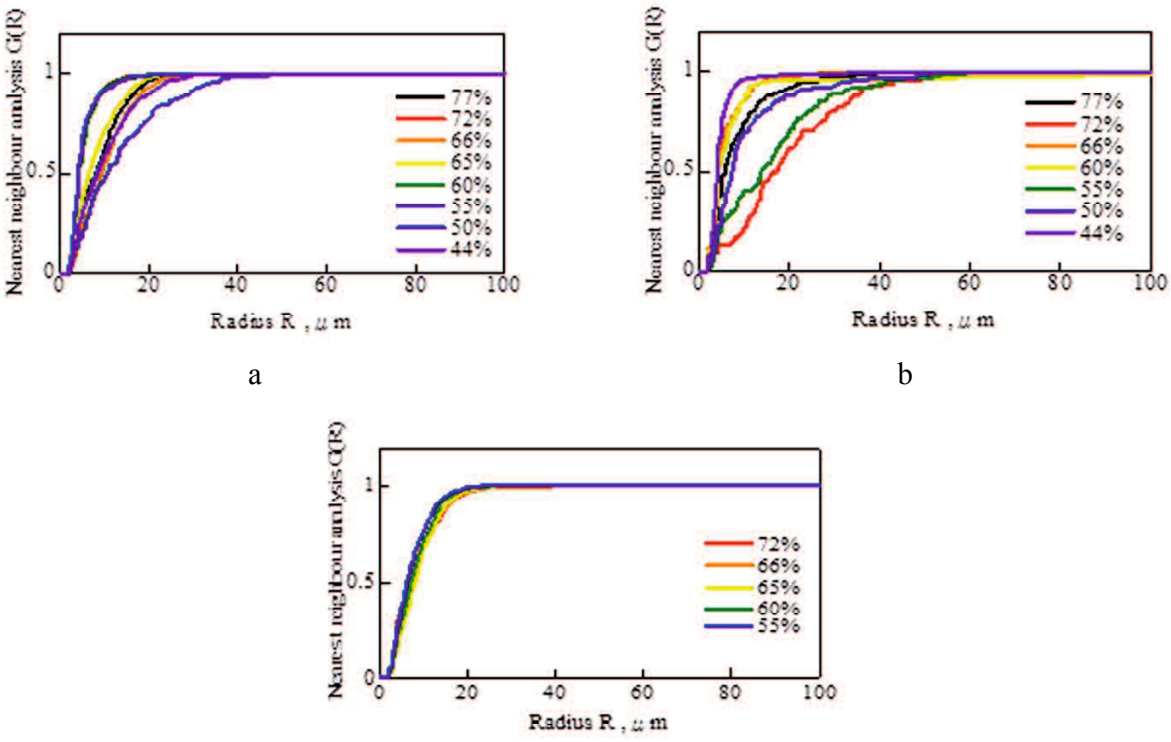

Fig. 2.20 $G(R)$ function analysis of nanoclay–epoxy composite specimens at a fatigue crack initiation area for (a) 1phr, (b) 3phr, and (c) 5phr.

$$G(R) = \frac{1}{n} \sum_{\substack{i=1 \\ d_i < R}}^{n} 1 \tag{1}$$

Here, the range of radius R from a nanoclay agglomerate centroid was set as 1–500 μm. In this calculation, the distance between agglomerates is given by the distance between gravity points of two corresponding agglomerates. The nearest neighbor distance d_i is defined by the shortest of all distances between the i-th agglomerate and other agglomerates (i=1, 2, …, n). In eq. (1) the count is performed when d_i is smaller than R, otherwise the count is not done, or it is zero. Figures 2.20a, b, and c respectively present results of the nearest neighbor analysis for 1phr, 3phr, and 5phr specimens. In these graphs, the abruptly rising slope of the shown graph exhibits

an uneven dispersion. In other words, it tends to have a higher clustering intensity of the nanoclay agglomerates compared to the gradually rising slope. The slopes in 5phr in Fig. 2.20c show a narrower range of the rising slope compared to the slopes of 1phr and 3phr specimens in Figs. 2.20a and b. This narrow range might result from the great amount of nanoclay in 5phr specimens, which increases the clustering effect at any parts of the specimen forming the rising slope similarly at any fatigue loading.

The correlation coefficients between $G(R)$ and the fatigue life deviation values were estimated for 1phr, 3phr, and 5phr specimens, and were added to Table 2.6. In this evaluation, the initial slope was substituted, which is obtainable by approximating all the data of $G(R)$ with a power law function. Here, a negative correlation coefficient more than 0.4 in absolute value defines that *G(R)* is a reasonable indicator to express the variation in fatigue life. Table 2.6 shows that all the results show negative correlation coefficients. Especially the coefficients of 1phr and 5phr are larger than that of a 3phr specimen. Although the correlation coefficient of 3phr specimens is not necessarily high, it might be said that the agglomerate clustering is related to the variation in fatigue life to some degree.

From this study, we were unable to find a highly reliable indicator that determines the relation between the fatigue life and agglomerates distribution state, but we understood the trend to approach the relation, i.e., the maximum size and the nearest neighbor function. Indeed, the quantitative analysis used for this study brings more objective direction in terms of understanding of the relation between the fatigue crack initiation and agglomerates. To achieve our final goal, more accumulation of experimental data and related statistical work must be done.

2.5 Conclusion

Fatigue tests of nanoclay-filled epoxy resin matrix composites were conducted. Then, the size and distribution state of nanoclay agglomerates were examined using an electron probe microanalyzer (EPMA).

I. The experimentally obtained results confirmed that the fatigue life decreased with an increase in nanoclay content. The 3phr and 5phr nanoclay-filled specimens showed a significant decrease compared to the neat specimen, whereas the 1 phr nanoclay-filled specimen was almost identical to the neat one.

II. Results of EPMA point analysis of the fatigue-fractured specimens revealed that more nanoclay agglomerates were present in the fracture surface than in the arbitrary cross-section.

III. Moreover, the EPMA area analysis showed that larger maximum agglomerates size was confirmed at the fatigue crack initiation area compared to other areas on the identical fracture surface. It can be estimated from such a quantitative analysis that a large-scale of agglomerates includes a weak interfacial bonding between clay layers, which causes the formation of numerous microcracks leading to fatigue crack initiation.

IV. In addition, the effect of interference between agglomerates was analyzed using the nearest neighbor function. The result demonstrates that, if the agglomerates exist more closely at the fatigue crack initiation area, then the fatigue life tends to decrease. Consequently, more closely stationed agglomerates cause fatigue crack initiation more readily.

Chapter III A Study on Fatigue Properties of Wood Filled Polypropylene Composites: Fabrication and Interfacial Adhesion

3.1 Introduction

The incorporation of natural fibers or wood flour into polymeric material creates new type of materials, i.e. potentially to be developed as an "environmentally friendly" material. In conjunction with this, recent and ongoing research on composite materials has put a focus on environmental aspect, as many related environmental problems occurred due to the usage of petroleum-derived materials and its difficulty to be recycled. Ito et al. [27] had proposed a new method in their study for compounding the Medium Density Fiberboard (MDF) waste and recycled resin from used package. This study shows a good example on handling waste materials such as MDF since MDF itself creates a huge problem for recycling industry regarding to its compositions. The obtained result indicates that the proposed method is sufficient and improved compared to the conventional method. As widely known, single wood materials has been used in many productions such as household articles, furniture and other interior items. The incorporation of wood flour into the polymer matrix gives an *extra* performance to the polymeric system itself. However due to the incompatibility of wood surface structure with the polymer matrix, the maximum performances of compounded wood flour in the composite materials are difficult to achieve.

From the literatures, the surface of the wood flour can be treated with sodium hydroxide, coupling with functional silanes, coating the wood fibers with stearic acid [10] or through a fibrillation process on the surface of wood fibers [28]. Commonly, the addition of functionalized

polymer such as maleic anhydride (MA) or acrylic acid (AA) into the polyolefin composites enhanced the performance of wood or natural based fillers inside the material. The functionalized polymer improves the interfacial adhesion between the wood with the hydrophobic polymer matrix. Here, the effect of grafting level of MA in maleated polypropylene has been investigated by Hristov et al. [11]. Three different amount of MA, 0.05 wt.%, 1 wt.% and 1.5 wt.%, was employed to wood/polypropylene (PP) by reactive extrusion in a single-screw extruder. It is reported that the addition up to 1 wt.% of MA amount was able to improve the tensile strength, elongation at break and impact strength of the wood/PP composite materials. Moreover, higher concentration of MA that was employed in compatibilizer results in reduction of ductility of the PP matrix. This study shows a good comparison on the formation of plastic deformation zone surround the wood particles at different MA concentration as characterized from the SEM image results. A study by Livia Danyadi et al. [10] compared the effect between larger molecular weight of maleic anhydried polypropylene (MAPP) and small molecular weight of MAPP on the tensile properties of the composite materials. The PP-MAPP-wood flour components were mixed in an internal mixer and compressed molded into a plate type specimens that used for tensile test and morphology observation. From this study, larger molecular weight and smaller functionality has been demonstrated to be more advantageous in order to improve the strength properties of the composite materials. Furthermore, the crystalline morphology of polymer and reinforcing wood flour is not influenced by compounding of coupling agent. In other words, the physical properties of components in composite materials are consistently retained even after the addition of MAPP. However, from this study, it is noted that the larger molecular weight of polymer exhibit higher viscosity and low melt index (MFI) characteristics, which turns to decrease the dispersion ability of wood flour in PP matrix. From the above literatures [10-12] on the usage of

coupling agent like MAPP into the wood/PP composites, it is understood that the incorporation of coupling agent enhances the adhesion aspect between PP matrix and the wood fiber surfaces.

In this chapter, the effect of MAPP amount on the fatigue properties of the wood-plastic composites (WPCs) will be discussed. For this purpose, different amount of MAPP was incorporated into the wood/PP composites. Consequently, the effect of different compounding process of MAPP was investigated by preparing two dissimilar types of specimens that are different in MAPP compounding process, namely as *process A* and *process B*, with fixed amount of wood flour, PP and MAPP. Then, the tensile and fatigue tests were carried out and finally further analysis on cross-sectional surface and fatigue fracture surface for all types of specimens was done to characterize the effect of MAPP on fatigue properties of WPCs.

3.2 Experimental methods

3.2.1 Materials

Polymer matrix used in this study was the random type PP pellet, J-3021 GR (melt mass-flow rate: 33 g/10 min, density: 900 kg/m^3 and antistatic feature) produced by Prime Polymer Co., Ltd. The wood flour, *Japanese Cedar* type thinned wood, was obtained from Ibi-forest Resource Utilization Centre, Gifu. The average size of the wood particles is around 5mm in length. Furthermore, a maleic anhydried polypropylene (MAPP) was added to the composites in order to improve interfacial properties of the materials. The emulsion type of MAPP, U-mex 1010 (solid content of 27%), produced by Sanyo Chemical Industries Ltd., was added at 1 wt.%, 2 wt.% and 5 wt.%, respectively.

3.2.2 Specimen fabrication

In order to investigate the effect of maleated polypropylene in wood filled polypropylene composite materials, four types of specimen were fabricated. The specimens were prepared with different amount of MAPP, in range of 1 wt.% to 5 wt.%. The final composition of various wood/PP composites are outlined in Table 3.1. In this study, two different processes were employed to compound MAPP into the wood flour. One was done by preblended MAPP with wood flour via pulverization process (*Process A*) and another is by compounding the MAPP after pulverized only the wood flour through the planetary ball mill (*Process B*). Generally, the materials were compounded as applied in Process B, however, Process A is designed to investigate the possible compounding method of MAPP for enhancing the interfacial bonding between the woods and polypropylene matrix. Flow chart for both processes are shown in Fig. 3.1 and Fig. 3.2 respectively. From these steps it could be inferred that different compounding

process exhibits opposites effects on the properties of the wood/PP composites. Hereinafter, the specimens are denoted as M1A, M2A, M2B and M5A, respectively.

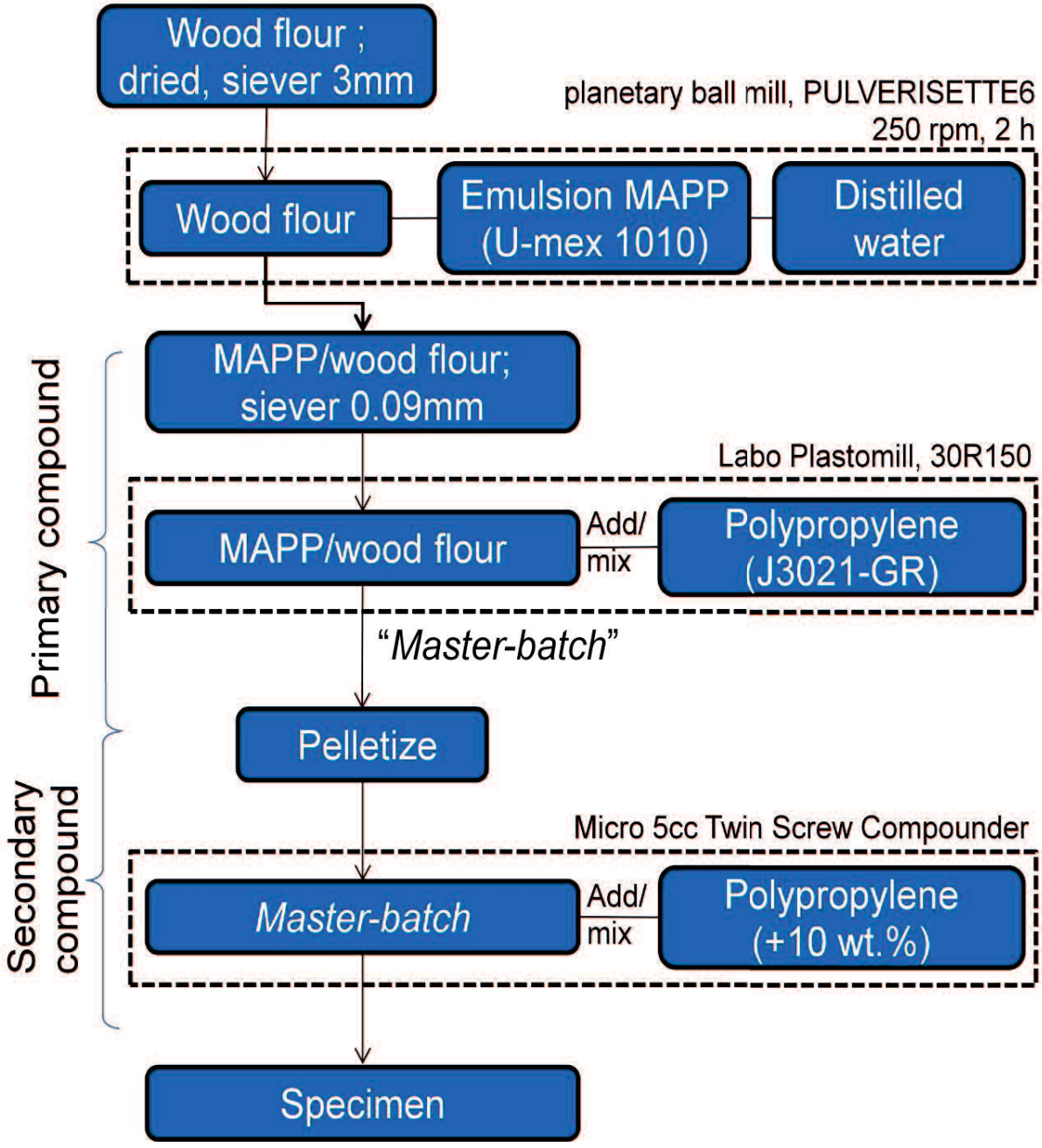

Fig. 3.1 Flow chart of Process A.

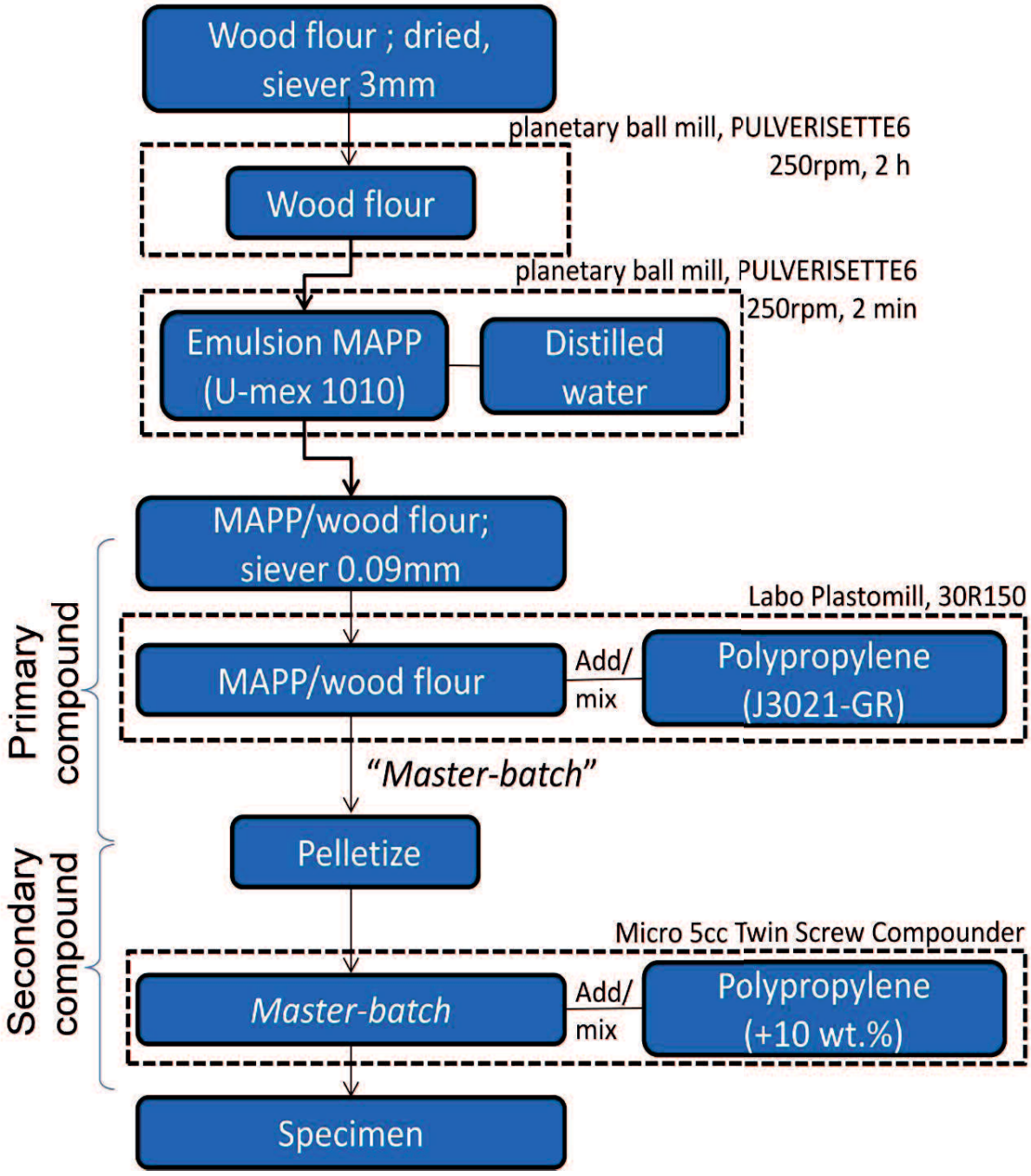

Fig. 3.2 Flow chart of Process B.

3.2.2.1 Process A

In order to reduce the water content of wood flour into below than 5%, it was first dried at 60 °C. Then, the wood flour was strained through a 3 mm mash-opening siever and added with the emulsion type of MAPP at 1 wt.%, 2 wt.%, and 5 wt.%, respectively. The mixture than was dried-pulverized in a 500 ml aluminum pot that contains 25 aluminum balls (ϕ20 mm) of a planetary ball mill machine (PULVERISETTE6; FRITSCH Japan Co.), as shown in Fig. 3.3, for 2 h at 250 rpm. The composition of the aluminum pot is one part mixture to one part free space and one part aluminum ball. At this stage, distilled water was added while mixing process in order to provided similar wt.% of MAPP mixture, i.e., to reduce the moisture effect on wood composite materials. By considering the frictional heat that may arise during the process, the pulverize process was stopped 1 min for every 10 mins. After that, the pulverized MAPP/wood flour was strained through a 0.09 mm mash-opening siever.

Kneading process was performed by dividing into two steps; primary and secondary compounding, for homogenization purpose and the specimen was molded through an injection molding machine after the secondary compound. For the primary compound, PP was added to the strained MAPP/wood flour and mixed together in the extrusion machine, Labo Plastomill (30R150; Toyoseiki Co.), as shown in Fig. 3.4, for 5 mins at 190 °C, 60 rpm. At this stage, the weight fraction composition of wood flour and MAPP-PP was 70 wt.% and 30 wt.% respectively. Here, the exact amount of PP is consequence to the added amount of MAPP as shown in Table 3.1. The primary kneaded mixture was pulverized into a small particle using a small crusher machine (Wonder Blender WB-1; Osaka Chemical Co.). Next, for the secondary compounding, another 10 wt.% of PP was added to the mixture and mixed well together through a small kneading machine Micro 5cc Twin Screw Compounder (DSM Explore Co.,) for 5 mins at

190 °C, 30 rpm. Finally, the specimens were molded into dumbbell shape via an injection molding machine Micro5, 5cc Twin Screw Compounder (DSM Explore Co.,). An overview of twin screw kneading and injection molding machine are shown in Fig. 3.5 and Fig. 3.6 respectively.

Fig. 3.3 Planetary ball mill machine.

Fig. 3.4 Labo Plastomill machine.

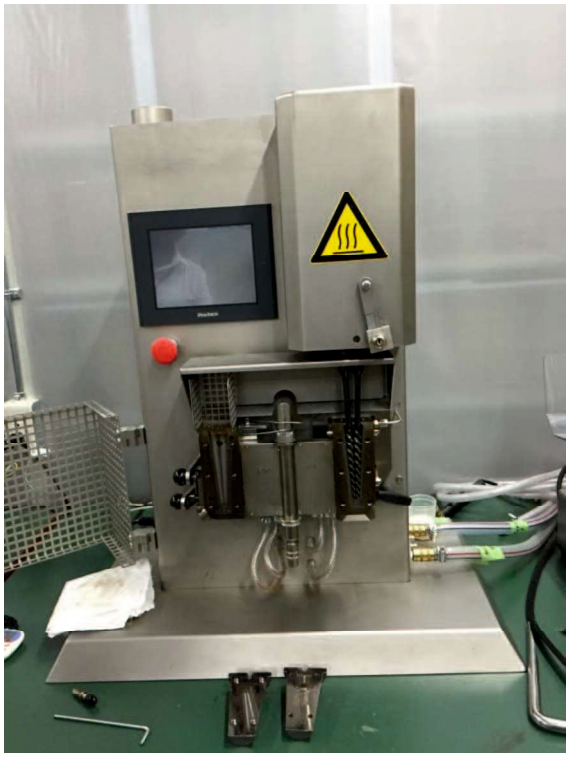

Fig. 3.5 Twin screw kneading machine.

Fig. 3.6 Injection molding machine.

3.2.2.2 Process B

As mentioned earlier, the difference between Process A and B is the compounding step of emulsion type of MAPP during the first pulverization process, i.e. in Process B, the MAPP was added after the wood flour had been pulverized with distilled water for 1 wt.% and 2 wt.% of MAPP mixture through the planetary ball mill.

First, the moisture content in wood flour need to be reduced to below than 5%, i.e. the wood flour was dried at 60 °C beforehand. Then, the wood flour was strained through a 3 mm mash-opening siever. The distilled water was added to the wood flour to provide similar liquid content for 1 wt.% and 2 wt.% of emulsion type MAPP mixtures and pulverized via the planetary ball mill for 2 h at 250 rpm with similar condition as mentioned in section 3.2.21. The process was stopped 1 min for every 10 mins to reduce the heat that generates from the friction during the mixing process. After that, the emulsion type of MAPP was added immediately and mixed for another 2 mins at 250 rpm. Then, the MAPP/wood flour was strained through a 0.09 mm mash-opening siever before the primary and secondary compound took place and finally the specimen was prepared by injection molding machine, Micro5, 5cc Twin Screw Compounder. The shape and dimension of the specimen for both process A and B are shown in Fig. 3.7.

Table 3.1 Composition percentage of wood fibers, PP and MAPP in composite material.

Specimens	**Wood fibers**	**PP**	**MAPP**
M1A	60	39	1
M2A	60	38	2
M2B	60	38	2
M5A	60	35	5

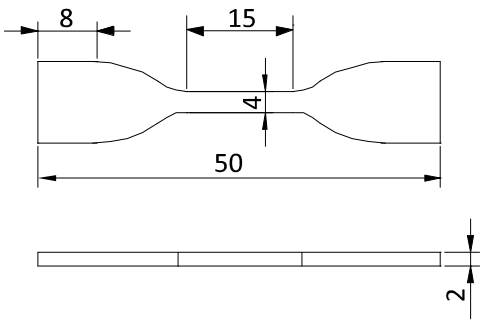

Fig. 3.7 Shape and dimension of each type of specimen.

3.2.3 Tensile and fatigue tests

A precision universal testing machine (Autograph AG-IS20kN; Shimadzu Corp.) was used to determine the tensile properties of each type of specimen. Tensile test was carried out at the crosshead speed of 50 mm/min up to fracture at room temperature. Meanwhile, the number of cycles to failure of each specimen was measured through a fatigue test using electric oil pressure servo type material testing machine (load capacity: 9.8 kN, Servo pulser EHF-FBI-4LA; Shimadzu Corp.,) at room temperature. The fatigue test was carried out at 50% to 80% levels of static fracture load obtained in the tensile test, and up to fracture or achieving 10^4 cyclic numbers. The stress ratio used here was 0.1 and the frequency was 1 Hz with sine wave.

3.2.4 Fracture surface observation

In order to understand the morphological structure of the wood/PP composite specimens at fracture area, the fracture surface of wood/PP composites from fatigue test was observed using the 3D Laser Measuring Microscope (LEXT OLS4000; Olympus Co.). Furthermore, the samples were observed at room temperature with 3 different objective lens, 20x, 50x and 100x,

respectively. The cross-sectional area of the WPCs specimens was observed using the scanning electron microscopy (SEM). The cross-sectional sample was prepared by embedded the specimen, that has been cut and polished at any cross-section area, into an epoxy-hardener solution in a silicon-case and hardened for 24 h at room temperature. Then, the observation surface was ground by using a grinding machine before it was polished. Finally, before the SEM observation, the golden vapor deposition was applied at the observation surface of the sample stage. Different amount of MAPP generates different characteristic of surface morphology of WPCs specimens. This can be confirmed by observing the cross-sectional area of the specimen.

3.3 Results and discussion

3.3.1 Tensile properties

As shown in Table 3.2, the strength and modulus of WPCs material increased with increasing MAPP amount as compared with Neat PP specimen. In comparison with the 1 wt.% of MAPP amount specimens, 2 wt.% and 5 wt.% of MAPP give about 18% and 22% higher strength and modulus properties, respectively. However, the different compounding processes, *process A* and *process B*, do not contribute much to the improvement of the tensile properties. This might be due to the similar compounding amount of MAPP. Hence, it is understand that the compounding of MAPP improved the interfacial bonding of wood interfacial surface with the hydrophobic polypropylene matrix, and thus, helps to transfer the shear load between wood flour. Such results support the arbitrary cross-sectional observation results (Figure 3.9) which indicates a good interfacial adhesion of higher MAPP amount specimen. Even so, Leu et al. [14] fixed the optimal amount of MAPP at 3 wt.%, along with the mass ratio of 50 wt.% wood fiber content, in which the fiber length was lower than 125 μm, comparable to that of the present.

Table 3.2 Tensile properties of Neat PP and WPCs specimens with different MAPP amount.

Specimens	Tensile strength [MPa]	Fracture load [N]	Young's Modulus [GPa]
Neat PP	31.7	-	0.84
M1A	32.2	281.2	1.54
M2A	35.3	308.0	1.67
M2B	34.9	309.2	1.61
M5A	37.9	331.1	1.88

3.3.2 Fatigue properties

Number of cycles to failure of each specimen was obtained from the fatigue test. From this result, the durability of the material under an arbitrary load can be estimated. Figure 3.7 illustrates the maximum stress to the number of cycles, so-called '*S*-*N* curves', for each type of specimen. All the regression lines were estimated by the least square method. From the diagram, the M5A specimens show the highest fatigue strength compared to M1A and M2A, M2B specimens, which indicated by the higher regression line. In other words, at any stress level of the *S*-*N* diagram, the specimens containing 5 wt.% MAPP show longer fatigue lives than those with lower MAPP contents. Meanwhile, similar regression lines are drawn-out on fatigue properties shown by both *process A* and *process B* specimens. However, the specimens fabricated through *process A*, M2A, indicates slightly higher number of cycles to failure, compared to that fabricated through *process B*. This might be because the commingling of wood fibers with the emulsion type of MAPP beforehand provides more suitable surface modification for matrix-filler bonding. The physical modification on celluloses of wood flour through the pulverization process attract the hydrogen bonding systems in cellulose to easily reacts with the MAPP molecules, thus provides better interfacial bonding between the woods and polymeric resin. The improved matrix-filler interfacial surface adhesion is believed to give higher fatigue resistance. As known from the comparison of Fig. 3.8 with Table 3.2, the similar result to the tensile test was also obtained in the fatigue test. Thus, it is concluded that higher MAPP amount, up to 5 wt.%, can improve the fatigue properties as well as tensile properties of WPCs specimens.

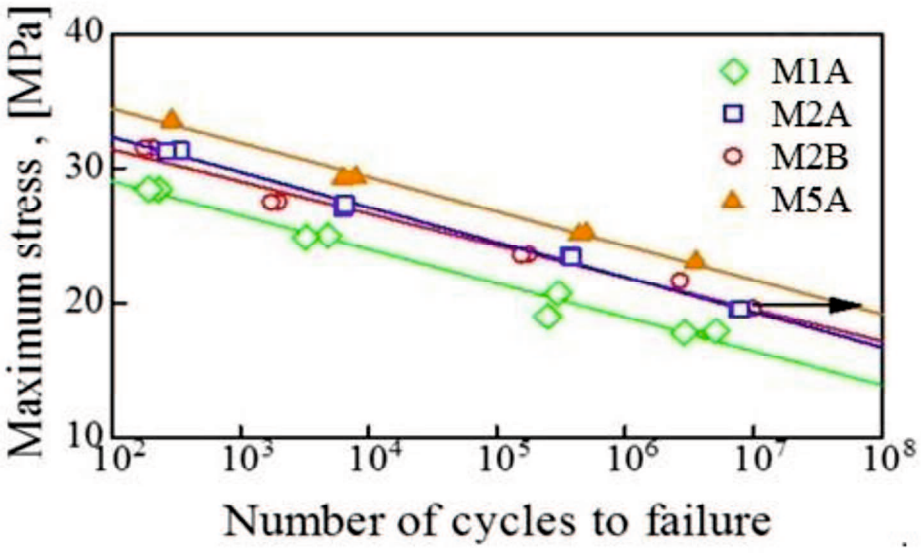

Fig. 3.8 S-N curves of each type of WPCs specimens.

3.3.3 Surface observation

As concerns the compatibility between the hydrophobic material of polymer material and wood flour, the addition of coupling agent is believed to give a better solution. The addition of coupling agent achieves chemically a strong interfacial bonding in a small quantity. Figure 3.9 indicates the observation results of SEM on WPCs specimen cross-sections with low and high amount of MAPP. At 1 wt.% of MAPP, the debonding areas between the wood flour and PP matrix are clearly observed as indicated by the red arrows, meanwhile at higher amount of MAPP (5 wt.%), most of the wood flour linked well with the polymeric resin. The debonding areas occur more largely around the larger size of wood flour compared to the small one. From the observation results, it is qualitatively characterized that higher amount of MAPP enhances the interface bonding between the hydrophilic wood flour and the hydrophobic polypropylene.

Fig. 3.10 shows the image result on fracture surface of each type of WPCs specimens, M1A, M2A, M2B and M5A, respectively. From these figures, it is understood that the fracture mechanism of each specimen, e.g. initial crack point and the crack propagation, is difficult to be observed. Moreover, from surface morphology, the fracture surface is independence from MAPP amount, i.e. Figs. 3.10a and b exhibit almost similar surface structure, that is unable to diffrentiate the MAPP amounts respectively. Hence, the plane structure of the fracture surface was ascertained to acquire surface information regarding to the fatigue crack initiation point.

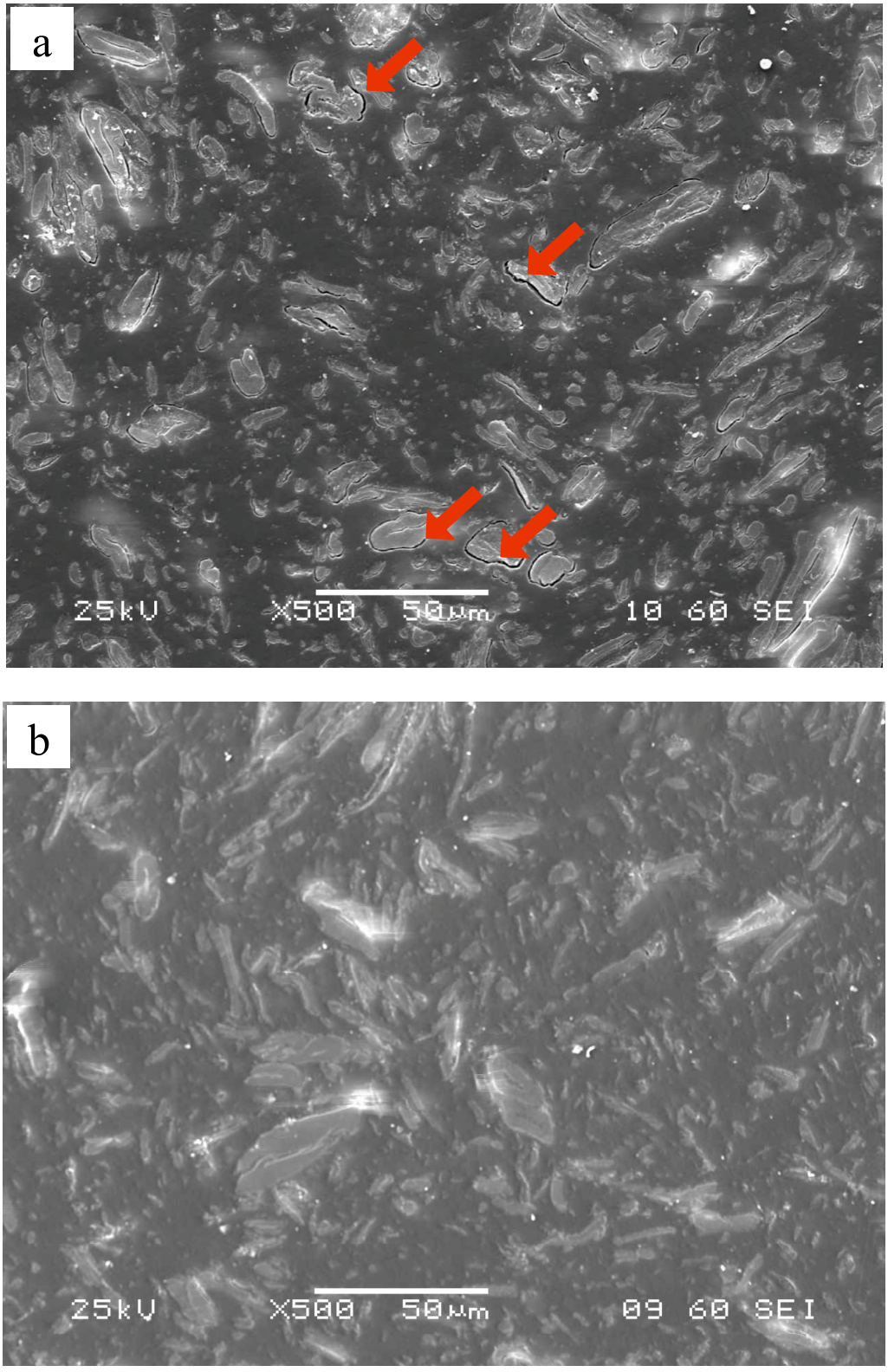

Fig. 3.9 Arbitrary cross-sectional of (a) M1A and (b) M5A specimens.

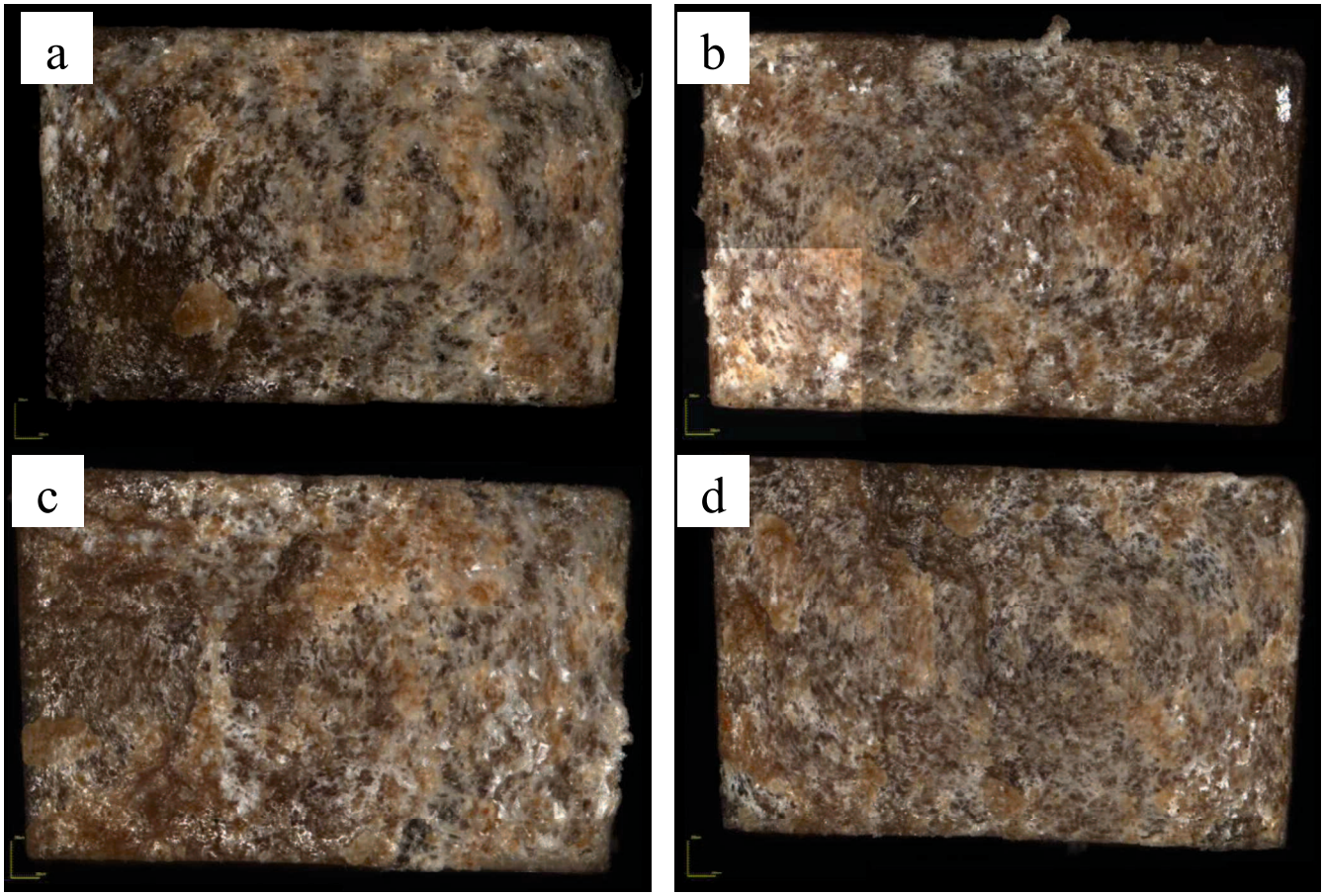

Fig. 3.10 Fracture surface of each type of WPCs specimens; (a) M1A, (b) M2A, (c) M2B and (d) M5A.

Figure 3.11 illustrates qualitatively the comparison of surface roughness of M1A and M5A specimens between the highest (80%) and lowest (55%) fatigue load, respectively. Here, specimens with higher fatigue load as illustrates in Figs. 3.11a and c demostrated rougher surfaces as compared to specimens with lower fatigue load (Figs. 3.11b and d). At higher fatigue load, the fracture surface morphology is close to the fracture behavior of tensile specimens. This is because the area of fatigue propagation plane is smaller, and therefore the rest of the area resembles tensile fracture surface at the final fatigue fracture, which end up with rough fracture surface. On the other hand, at lower fatigue load, the fracture surface exhibit less rough surface, i.e. a flatter surface as shown in Figs. 3.11b and d. At a point, the flat surface at lower fatigue

load specimens exhibits the behavior of crack propagation from the initial area, which is will be discussed in more detail in Chapter 4 on determination of failure behavior of WPCs material.

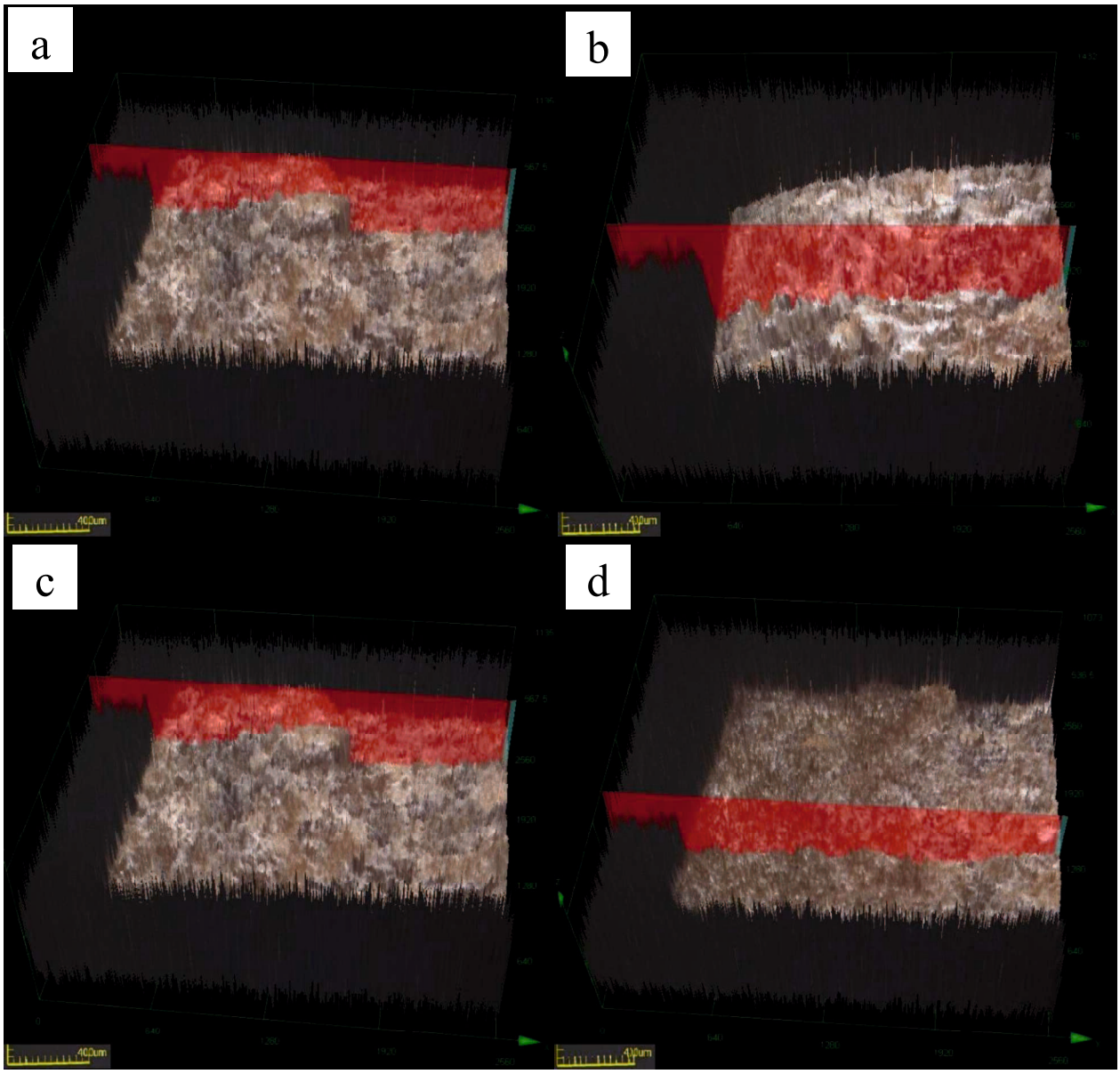

Fig. 3.11 Surface roughness of (a) M1A at 80% fatigue load, (b) M1A at 55% fatigue load, (c) M5A at 80% fatigue load and (d) M5A at 55% fatigue load, respectively. (The lower border of the red area shows the surface roughness)

3.4 Conclusions

In this study, different amount of MAPP was mixed with PP matrix and wood flour to form a wood/PP composite material. The effect of MAPP amount on fatigue properties of wood/PP composite material was investigated.

I. From the experimental tests, each of the tested specimen demonstrates the similar pattern for both tensile and fatigue properties. Up to 5 wt.% of MAPP amount had increased the tensile strength, Young's modulus and fatigue life of M5A specimens, meanwhile decreasing with the reduction of MAPP amount, respectively. That is to say, the improvement of these properties is dependent on the increment of MAPP amount.

II. From tensile properties, the diference between Process A and Process B was not clearly identified, however, it is understand that from the S-N diagram of fatigue result indicates the improvement in fatigue life of specimens fabricated from Process A as compared with that of Process B.

III. From the observation on morphology of each specimens, the fracture behavior of wood/PP composite was not clearly observed, regardless to the MAPP amount. However, the surface roughness observation at higher and lower fatigue load denote a hint on determining the fracture behavior of WPCs material.

Chapter IV Evaluation of Fatigue Fracture Behavior of Wood Filled Polypropylene Composites

4.1 Introduction

Appropriate amount of fillers and the compatibility of woods with the hydrophobic polymer are among the issues that have been discussed as the significant factors for improving the properties of the wood-plastic composites (WPCs) material. Other factors that may be related to the improvement of the WPCs are listed as follows:

i. **Fillers distribution -** short fibers and particulates type's fillers tend to agglomerate and formed into clusters. The formation of agglomerates and clusters is less favorable for any fabrication process of composite materials which results in higher stress concentration at the local area of the clusters. Higher stress concentration will initiates a micro-crack upon the premature failure of the composite materials.

ii. **Fillers conditions -** the different size of the wood fibers gives variety in the performance of the WPCs [14, 29]. Larger size of wood fibers might increase the moisture content inside the WPCs, thus increase the moisture absorption ability and affect the properties of the material. Fibrillization of the wood fibers is also one of the methods to improve the performance of WPCs since the entanglement in between the wood fibers and the matrix had increased.

The study on optimization of the materials and its conditions of WPCs had been carried out [14] in order to obtain optimal conditions for fabrication purpose. However, the effects of the

optimization conditions regarding to the durability of the materials and its failure mechanism have not been discussed.

In this chapter, different amount of wood flour was employed to wood filled polypropylene (PP) composites in order to clarify the effect of the fillers amount on the fatigue properties of the WPCs. Moreover, a study on the fracture surface of the fatigue test specimens had been carried out to provide related information regarding to the fatigue failure behavior of WPCs. Here, the dried WPCs pellets that are relatively containing higher amount of wood fillers than the polymer matrix were mixed with the dried PP pellets through an extrusion process and molded by the injection molding machine. The tensile and fatigue tests were carried out for each type of specimen to examine the influence of wood fibers amount on tensile and fatigue behavior of WPCS. Consequently, further analysis on cross-sectional area of the specimen and fatigue fracture surface has been carried out and the relation between microscopic fracture and the fatigue behavior will be further discussed in this chapter.

4.2 Experimental methods

4.2.1 Materials

In this study, WPCs specimens with different weight fraction of wood flour were prepared by using *master-batch* pellets (CELBRID N, wood fiber length 150 μm; TOCLAS Corp.). The pellets were mixed with J107G type polypropylene (Homopolymer, MI=30; Prime Polymer Co.) by using a single screw extruder machine in order to gain desired weight fractions of wood flour. Figure 4.1 shows the overview of master-batch pellets and J107G type polypropylene.

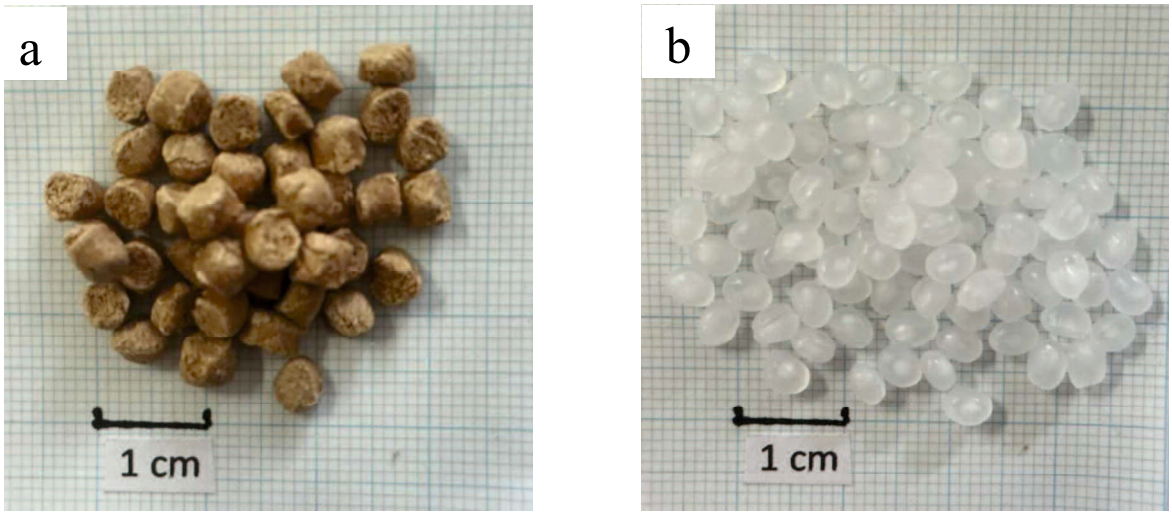

Fig. 4.1 Overview of (a) master batch pellets and (b) J107G type polypropylene pellets.

4.2.2 Specimen fabrication

To investigate the effect of wood composition in WPCs specimens on fatigue behavior, different composition of WPCs specimens were fabricated through an extrusion and injection molding processes. The PP and *master-batch* pellets were first dried in a convection oven (MOV-112F; Sanyo Co.) at 120 °C for 5 h to reduce the moisture contents. Then, a desired amount of dried PP was added and mixed together with the dried *master-batch* pellets that

caused a reduction of wood flour weight fraction to a desired amount as mentioned above. The mixing process was done using a single screw extruder machine (Musashino Kikai Co. Ltd.) as shown in Fig. 4.2. Here, the mixing conditions need to be set first in order to obtain material properties that produce maximum performance. For this purpose, first, the WPCs specimens with 30 wt.% of wood flour weight fraction were fabricated under different mixing temperatures; 180 °C and 190 °C, and screw's speed of 5 rpm, 10 rpm, 20 rpm and 30 rpm, respectively. The extrusion process was done twice at same temperature and speed for each type in order to acquire an optimum dispersion of wood flour. After that, the extruded mixture was chopped into 5 mm length pellet before molded into a dumbbell shape via an injection molding machine (Fig. 4.3) at 200 °C. A static tensile test was carried out to each type of specimen and the optimum mixing conditions were selected from the tensile test results.

After the mixing conditions were recognized, under a similar mixing conditions and process, the specimen with 50 wt.% of wood flour were fabricated to investigate the influence of wood flour amount on tensile and fatigue properties of WPCs. In addition, the effect of the dispersion of wood flour was examined by comparing the specimen's properties that were fabricated under different number of extrusion processes, i.e. single and double extrusion processes. These specimens are denoted as 30%WF/PP-1, 50%WF/PP-1 and 30%WF/PP-2, 50%WF/PP-2.

As for the neat PP specimen, the dried PP pellets were directly added into the injection molding machine and molded under the same condition with WPCs specimens. The shape and dimension of both Neat PP and WPCs specimens are shown in Fig. 4.4. The specimens were stored for at least 24 h before the tensile and fatigue tests were carried out. The mixing conditions and type of specimens are summarized in Table 4.1and Table 4.2, respectively.

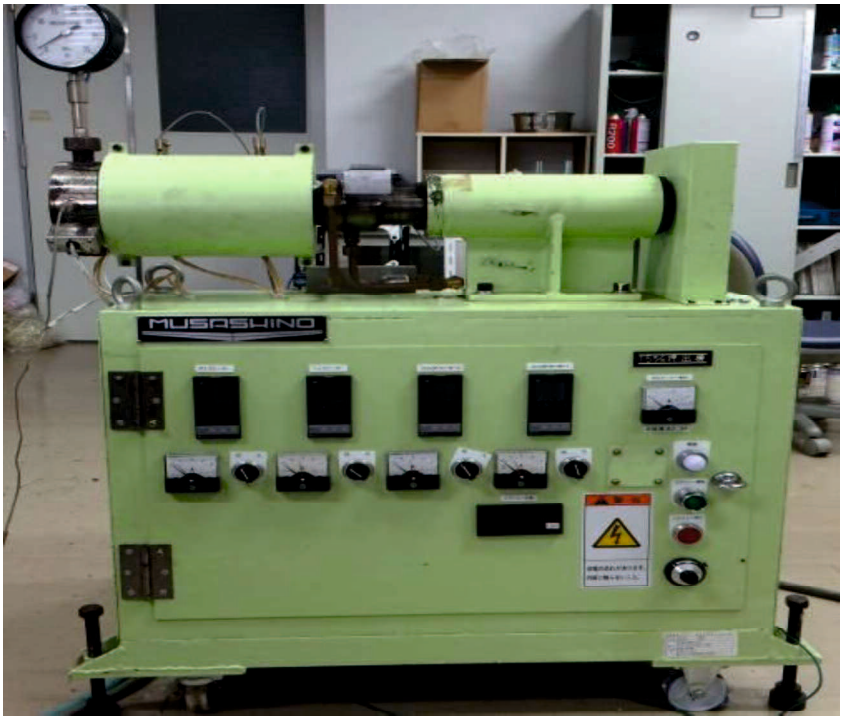

Fig. 4.2 Overview of single screw extruder machine.

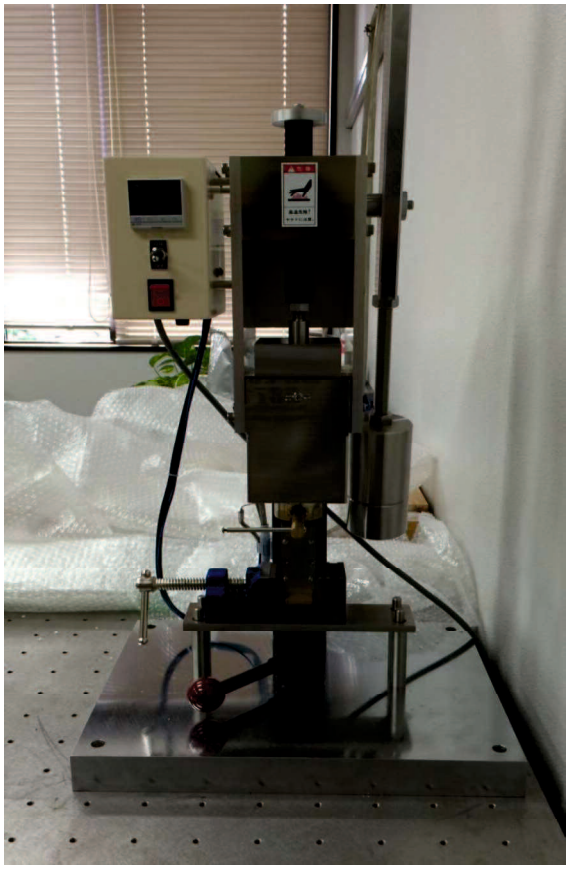

Fig. 4.3 Overview of injection molding machine.

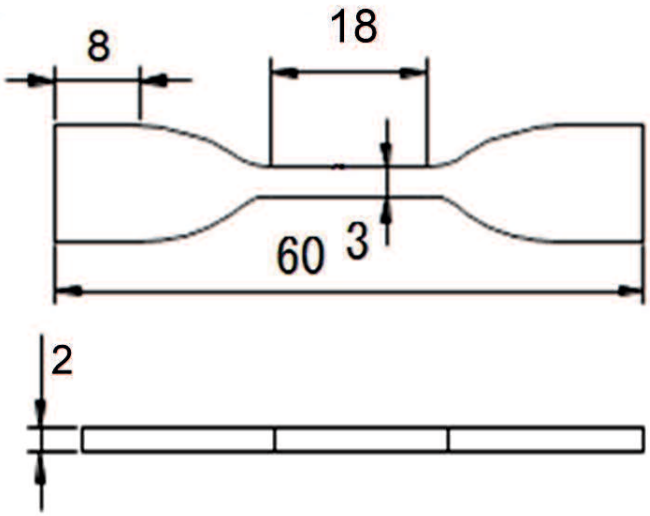

Fig. 4.4 Shape and dimension of neat and each type of WPCs specimens.

Table 4.1 Different mixing conditions of WPCs specimens.

Temperature [°C]	Screw speed [rpm]	Number of specimens
180	5	5
	10	7
	15	9
	20	9
190	5	7
	10	9
	15	9
	20	5

Table 4.2 Compositions and types of WPCs and Neat PP specimens.

Specimens	PP [%]	Wood fibers [%]	Number of extrusion process
Neat PP	100	-	-
30%WF/PP-1	70	30	1
50%WF/PP-1	50	50	1
30%WF/PP-2	70	30	2
50%WF/PP-2	50	50	2

4.2.3 Tensile and fatigue tests

A small-type tabletop testing machine (LSC-1/300; JT Tohsi INC.) was used to determine the tensile properties of neat PP and WPCs specimens. The overview of the tabletop testing machine is shown in Fig. 4.5. A strain amplifier (DPM-700B; Kyowa Electronic Instruments Co.

Ltd.) and a strain gauge (KFG-2N-120-C1-11; Kyowa Electronic Instrument Co. Ltd.) were used for strain measurements during the tensile test. Tensile tests were conducted at a crosshead speed of 10 mm/min up to fracture at room temperature. The number of cycles to failure of each type specimen was measured through a fatigue test using an electric oil pressure servo type material testing machine (9.8 kN load capacity, Servo pulser EHF-FBI-4LA; Shimadzu Corp.) at room temperature. The fatigue test was conducted at 50%–80% levels of static fracture load, obtained from the tensile test, up to fracture or achieving more than 10^6 cyclic numbers. The stress ratio used in this study was 0.1 and the frequency was set at between the ranges of 1 Hz to 5 Hz, respectively.

Fig. 4.5 Overview of tabletop tensile testing machine.

4.2.4 Fracture surface observation

In order to understand the morphological structure of the wood filled polypropylene composite specimens at fracture area, the fracture surface of composite specimens from fatigue test was observed using the scanning electron microscope (SEM) as shown in Fig. 4.6. The fracture surface sample was prepared by cutting the fractured specimens into 5 mm in length and the golden vapor deposition was conducted at appropriate thickness for each sample using micro-ion weld slag equipment. On the other hand, the wood flour distribution was observed from the arbitrary cross-sectional area of the specimen. The cross-sectional sample was prepared by embedded the specimen, that has been cut and polished at any cross-section area, into an epoxy-hardener solution in a silicon-case and hardened for 24 h at room temperature. Then, the observation surface was ground by using a grinding machine before it was polished. Finally, before the SEM observation, the golden vapor deposition was applied at the observation surface of the sample stage. Besides SEM, the fracture surface area was also observed using the 3D Laser Measuring Microscope (LEXT OLS4000; Olympus Co.). The samples were observed at room temperature with three different objective lens, 20x, 50x and 100x, respectively.

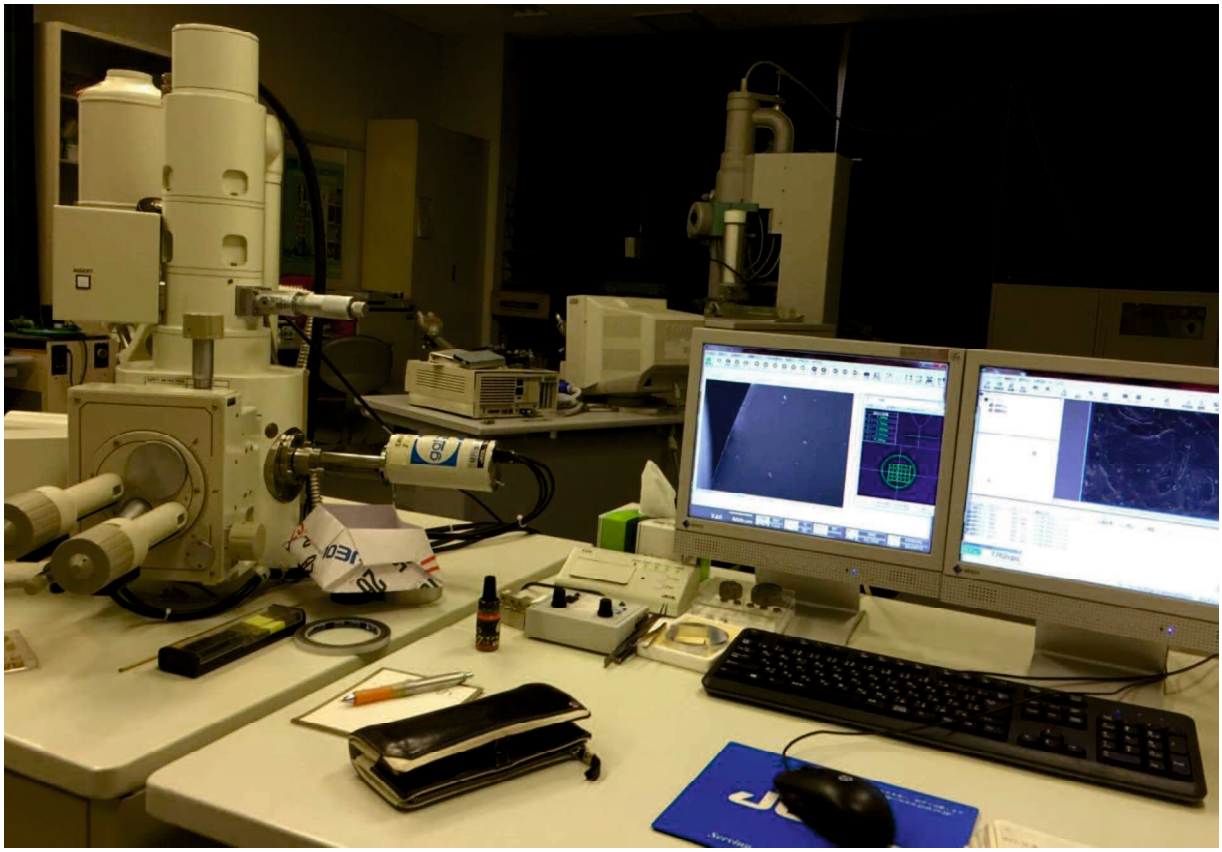

Fig. 4.6 Overview of scanning electron microscopy (SEM) machine.

4.3 Experimental Results

4.3.1 Optimal fabrication conditions

As mentioned in section 4.2.2, the optimum mixing conditions, i.e., mixing temperature and screw's speed, were investigated. Figure 4.7 illustrated the average tensile strength of each specimen according to the predefined mixing conditions. Here, it is understand that the tensile strength was slightly increased for specimens that were fabricated at 190 °C compared to that of with 180 °C as the mixing temperature. For specimens with mixing temperature of 190 °C, the tensile strength was slightly improved for specimens with screw's speed of 10 rpm to 20 rpm,

however, to some extent decreased at 5 rpm and 30 rpm. At higher screw's speed, the mixing time become shorter where sufficient kneading cannot be obtained, meanwhile the mixing time become longer at low screw's speed; result in thermal degradation of WPCs material. In another words, it is considered that the improper kneading that leads to the poor distribution of wood fiber and thermal degradation of the material contribute to the declination of the tensile strength. Thus, in this study, the optimal mixing condition was set at 190 °C and screw's speed of 20 rpm, and this condition was applied for the rest of the fabrication process.

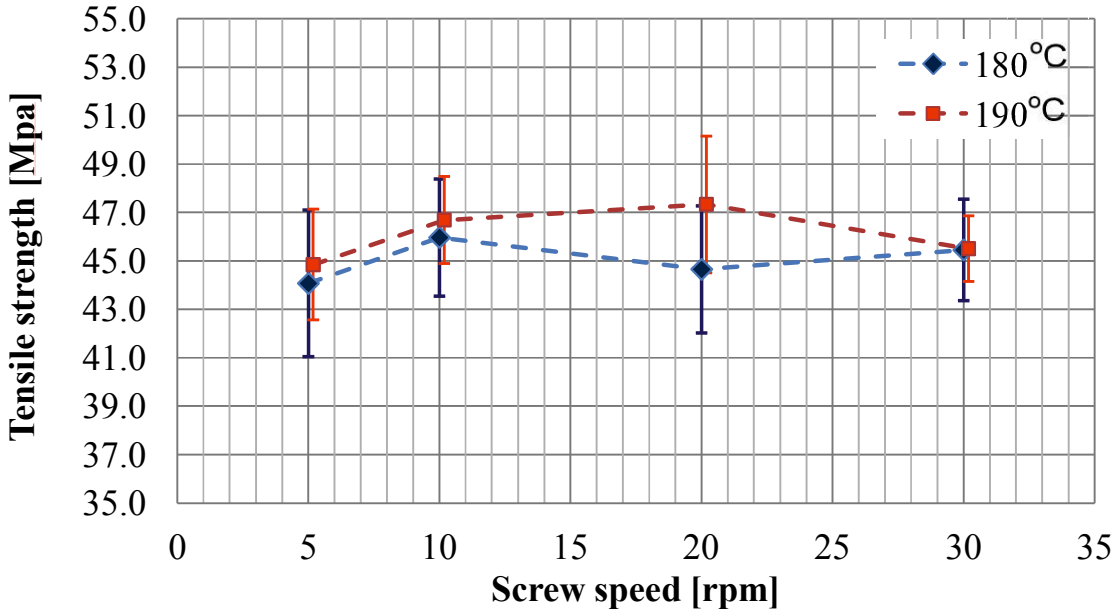

Fig. 4.7 Average tensile strength of each specimen according to the predefined mixing conditions.

4.3.2 Tensile properties

Figure 4.8 illustrates the stress-strain diagram of representatives for neat PP and WPCs specimens. From the tensile test result, it is understood that the tensile strength and Young's modulus of PP material improved by compounding the wood fibers into the PP matrix. Table 4.3 shows the average value of tensile properties of Neat PP, 30 wt.% and 50 wt.% of wood composition in WPCs specimens. As shown in this table, the tensile strength and Young's modulus properties increased with increasing the weight fraction of wood fibers. Moreover, it is understand that, by compounding 30 wt.% of wood fibers into the PP matrix, the strength and modulus of the materials showed about 22% and 75% increases, respectively, and both properties increased up to 51% and 135% for 50%WF/PP specimens.

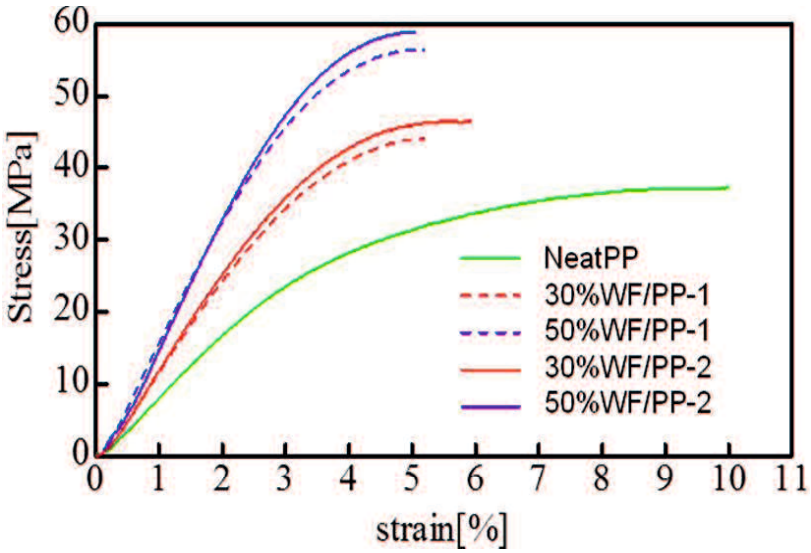

Fig. 4.8 Stress-strain diagram of neat PP and WPCs specimens.

Table 4.3 Average value of tensile properties of Neat PP and WPCs specimens.

	Number of samples	Tensile strength σ [Mpa]	Strain at break ε[%]	Young's Modulus E [GPa]
Neat PP	5	38.2	10.02	2.00
30%WF/PP-1	5	44.1	5.52	3.87
50%WF/PP-1	5	55.9	5.08	4.79
30%WF/PP-2	12	46.5	5.89	3.49
50%WF/PP-2	6	57.7	4.94	4.70

4.3.3 Fatigue properties

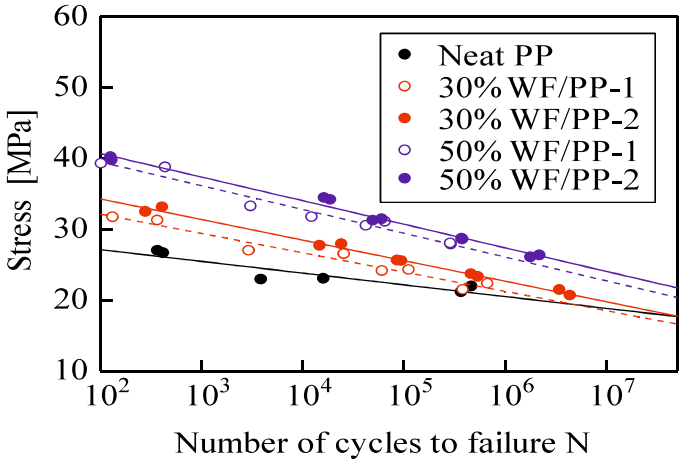

Fig. 4.9 S-N curves of Neat PP and WPCs specimens.

Number of cycles to failure of each specimen was obtained from the fatigue test. From this result, the durability of the material under an arbitrary load can be estimated. Figure 4.9 illustrates the maximum stress to the number of cycles, so-called '*S-N* curves', for neat PP specimen and WPCs specimens with different wood fibers weight percentages. As compared to Neat PP specimen, the WPCs specimens tend to be fractured at lower number of cycles when the

specimens are subjected to higher ratio of fatigue load. On the other hand, the fatigue strength was improved by mixing the wood fibers into the PP. Higher weight fraction of wood fibers can exhibit higher fatigue strength. Regarding the specimens with single and double extrusion processes through the single screw extruder machine, the dispersion state of wood fibers in the latter was clearly better than the former, as shown later. As seen in Fig. 4.9, both WF/PP-2 specimens indicate higher fatigue properties compared to the WF/PP-1 specimens.

4.4 Discussion

4.4.1 Cross-sectional and fracture surface observation

Figure 4.10 shows an arbitrary cross-sectional area of 30%WF/PP and 50%WF/PP specimens at single and double extrusion processes. The clustered wood fibers are clearly seen in Figure 4.10a, of which the largest cluster size is approximately 600 μm in length. When high amount of PP was added to the highly dense wood-PP pellets (CELBRID N; *master-batch* pellet contains approximately 70 wt.% of wood fibers), it is hard for the pellets to disband and scatter uniformly through the PP matrix in a short time. That is to say, the duration of single extrusion to mix the materials is considerably short, resulting in the formation of clustered wood fibers as mentioned in section 4.3.1. Unlike 30%WF/PP-1 specimens, 50%WF/PP-1 causes the formation of smaller clusters because of less amount of PP mixed with *master-batch* pellets, as shown in Fig. 4.10b. Figures 4.10c and d show arbitrary cross-sections of 30%WF/PP-2 and 50%WF/PP-2 specimens. The wood fibers were distributed at more favorable distribution level, leading to the good results for both tensile and fatigue tests.

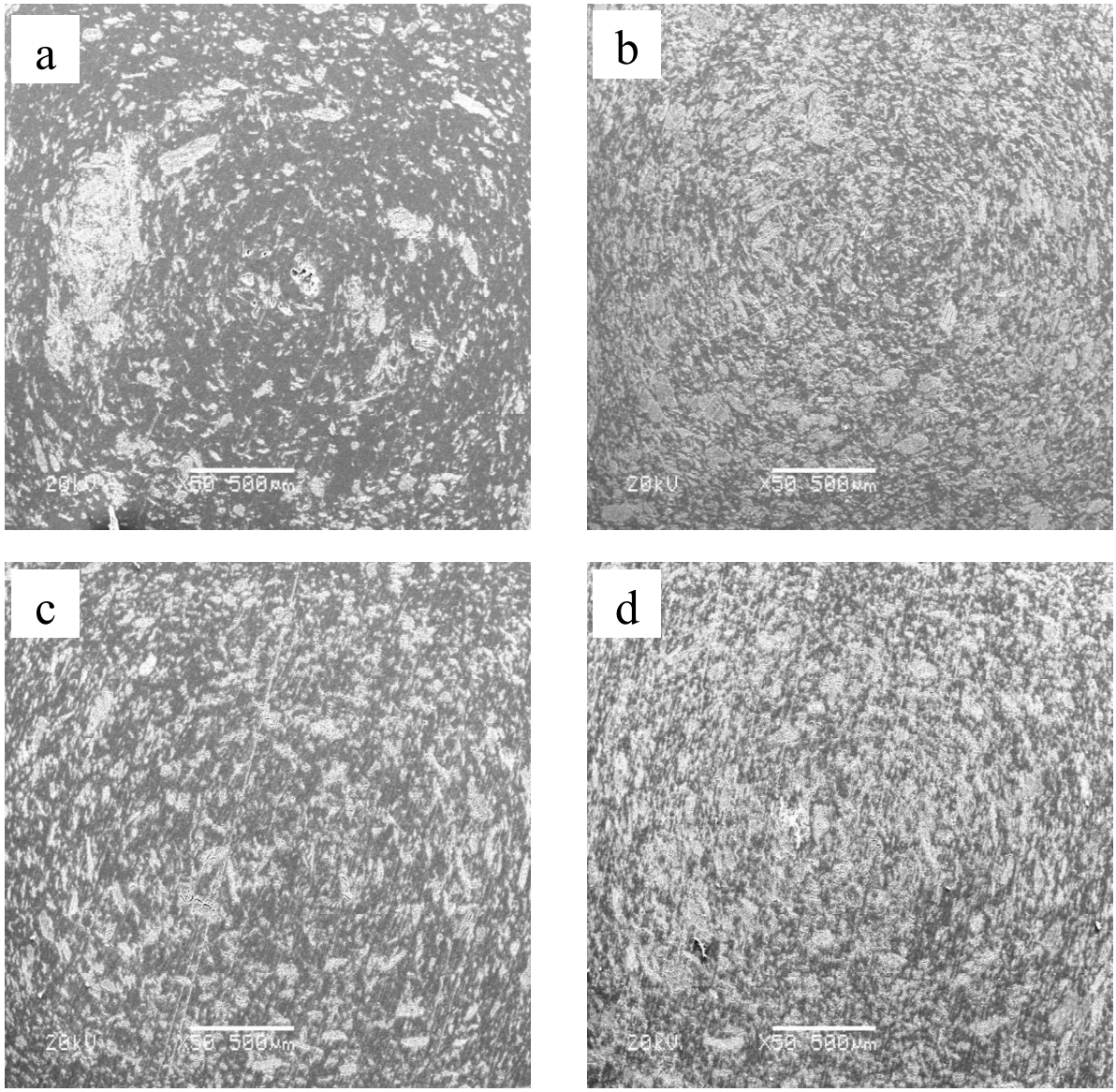

Fig. 4.10 Observation of cross-sections of (a) 30%WF/PP-1, (b) 50%WF/PP-1, (c) 30%WF/PP-2 and (d) 50%WF/PP-2 specimens.

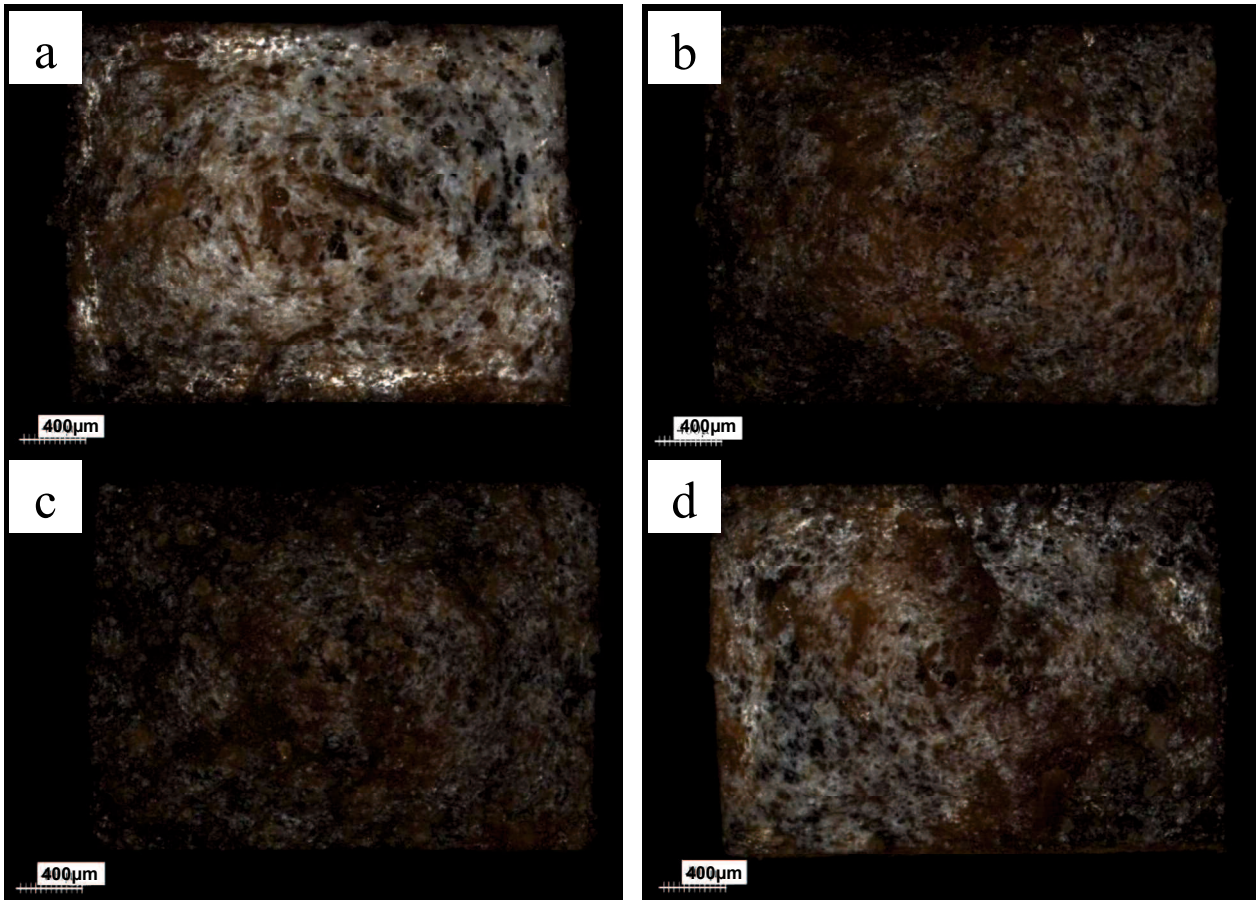

Fig. 4.11 Fatigue fracture surface of each type of WPCs specimens at 70% of fatigue load: (a) 30%WF/PP-1, (b) 50%WF/PP-1, (c) 30%WF/PP-2 and (d) 50%WF/PP-2.

As for metal-based materials, the fatigue behaviors from the fatigue fracture surface are much easier to recognize compared to the WPCs material. This is because, the fatigue damage process that are commonly found at the fracture surface of the metallic materials, such as crack nucleation area, crack propagation path, striation and so on, are somehow almost impossible to mark out at WPCs surface. Consequently, the fatigue behaviors of this material are difficult to be characterized. As shown in Figs. 4.11a - d, the fatigue fracture surface of each type WPCs specimen exhibits non-specific patterns of fatigue behavior, independent of the number of extrusion or the weight fraction of the wood fibers. Furthermore, the similar morphology was

observed independent of fatigue load levels. As mentioned above, the fatigue behavior is commonly traced at the fracture surface, but it is definitely difficult to clarify the trace in detail.

4.4.2 Fatigue damage of WPCs and failure mechanism

An observation method was set up in order to understand the fatigue behavior of WPCs specimens. Firstly, a short-length video was taken at certain time before the specimen reached to fracture. The whitened area that was formed after a certain number of cyclic loading and fatigue load level was observed from the area nearby the side surface of the specimen, as indicated by the arrow of Fig. 4.12a. After that, the whitened area extended toward the center of the specimen, as shown in Fig. 4.12a, and finally the specimen was fractured. The horizontal plane of fatigue fracture surface of the specimens was then examined by 3D Laser Measuring Microscope to confirm the difference of physical and morphology between the area close to the crack initiation and the remote area from the initiation point. From Fig. 4.12b, it is understood that the fatigue fracture surface of WPCs specimen contains different surface morphologies and color. One is a relatively flat surface, and another shows an uneven surface. And the former consists of the whitened area, and the latter is a brown area which is the WPCs' original color. That is to say, the former surface is corresponding to the stable crack propagation area despite the non-opening and the latter is to the unstable one. Although it is estimated that the whitened area is caused by crazing of PP matrix, this area behaves as a crack.

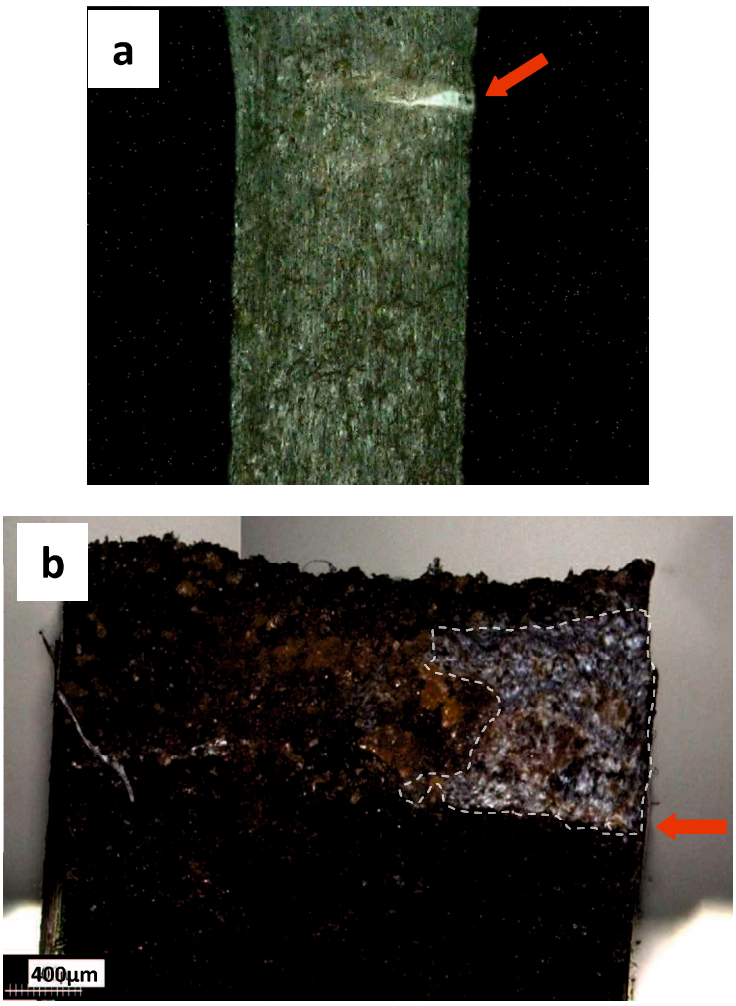

Fig. 4.12 (a) Fatigue crack initiation area (indicates by arrow) before the specimen ruptured at certain number of cyclic loading; (b) fatigue fracture surface contains different morphologies and color.

The good interfacial adhesion of matrix-fillers increases the deformation resistance of the material, but at the specimen surface, PP matrix tends to deform largely compared to the inside because of free surface. This leads to occurrences of the plastic deformation or micro-cracks for PP matrix surround the wood fibers, while internal PP matrix is restricted in deformation and expansion stress occurs without crack extension, especially at the area nearby the plastic deformation or micro-cracks area (Fig. 4.13a). Expansion stress occurring in the matrix causes

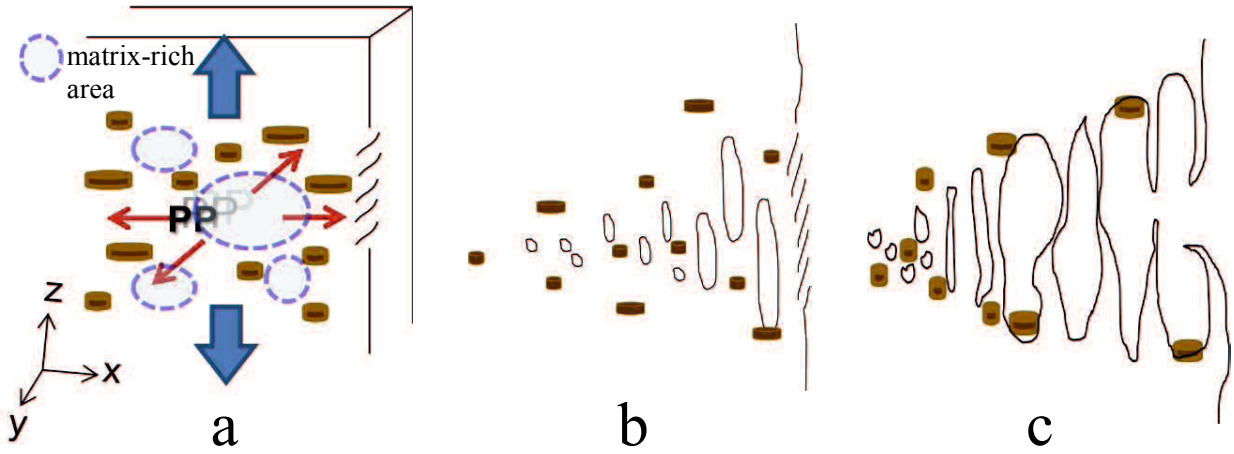

Fig. 4.13 Schematic figure of fatigue fracture behavior of WPCs specimen.

micro-voids and followed by fibrillation of PP molecular chains as shown in Figs, 4.13b and c. We consider this is the mechanism of whitening, i.e. crazing, at the fatigue damage process. Moreover, crazing extends into the polymer-rich area in between wood fibers, under cyclic loading. Even if wood fibers exist ahead the tip of the crazes, crazing extends without involving wood fibers, because the fibers adhere at the root of fibrillation due to the strong bonding. Thus, at the craze extension area, many traces of PP matrix fibrillation are observed, as shown in Fig. 4.14a, and also some wood fibers are recognized. This aspect is clearly different from the unstable propagation area illustrated in Fig. 4.14b.

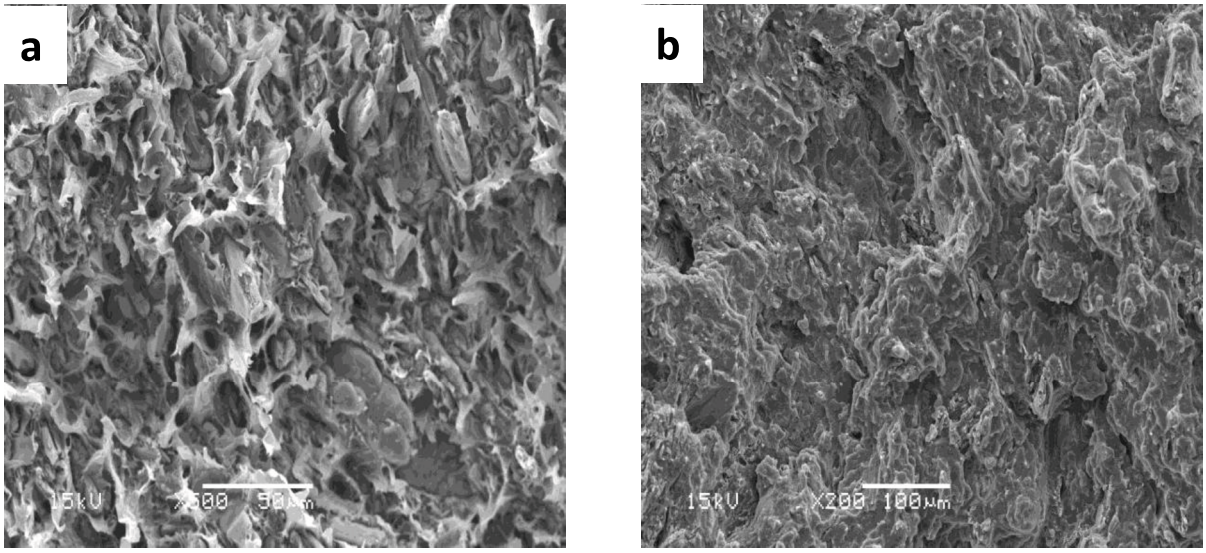

Fig. 4.14 Fatigue fracture surface at (a) nearby the crack initiation area and (b) unstable propagation area.

4.5 Conclusions

In this study, different weight fractions of wood fibers in WPCs specimens were fabricated in order to investigate the influence of wood fibers weight fraction on the tensile and fatigue properties.

I. From the this study, the tensile and fatigue properties of WPCs were enhanced by compounding the wood fibers up to 50 wt.%. The good interfacial adhesion between the wood fibers and the PP matrix, as a result from the addition of coupling agent MAPP to the compound, plays an important role towards enhancing the properties of WPCs material.

II. In addition, the dispersion of wood fibers inside the PP matrix was improved through the double extrusion process.

III. From the fatigue fracture surface observation, it was conclude that the fatigue damage mechanism of WPCs specimen was initially formed by a plastic deformation or micro-crack at specimen's surface area and then continued to bring the crazing process toward the inside of the specimen until finally a catastrophic failure occurred.

Chapter V Summary

Fatigue properties of nanoclay nanocomposites and wood filled polypropylene composite materials were investigated. Moreover, the fatigue fracture behavior was characterized from the fatigue fracture surface. Based on the results of the present study, the conclusions can be summarized as follows.

In Chapter II, the neat epoxy matrix and nanoclay-epoxy (NE-) composites specimens were prepared with different nanoclay amount to investigate the influence of the nano-size fillers amount to the fatigue properties and the fatigue fracture behavior was evaluated from the observation at fracture surface area. The experimentally obtained results confirmed that the fatigue life decreased with an increase in nanoclay content. The 3phr and 5phr nanoclay-filled specimens showed a significant decrease compared to the neat specimen, whereas the 1 phr nanoclay-filled specimen was almost identical to the neat one. Results of EPMA point analysis of the fatigue-fractured specimens revealed that more nanoclay agglomerates were present in the fracture surface than in the arbitrary cross-section. Moreover, the EPMA area analysis showed that larger maximum agglomerates size was confirmed at the fatigue crack initiation area compared to other areas on the identical fracture surface. It can be estimated from such a quantitative analysis that a large-scale of agglomerates includes a weak interfacial bonding between clay layers, which causes the formation of numerous microcracks leading to fatigue crack initiation. In addition, the effect of interference between agglomerates was analyzed using the nearest neighbor function. The result demonstrates that, if the agglomerates exist more closely at the fatigue crack initiation area, then the fatigue life tends to decrease. Consequently, more closely stationed agglomerates cause fatigue crack initiation more readily.

In Chapter III, the effect of coupling agent MAPP amount on fatigue properties of WPCs was investigated. From the experimental tests, each of the tested specimen demonstrates the similar pattern for both tensile and fatigue properties. Up to 5wt% of MAPP amount had increased the tensile strength, Young's modulus and fatigue life of M5A specimens, meanwhile decreasing with the reduction of MAPP amount, respectively. That is to say, the improvement of these properties is dependent on the increment of MAPP amount. From tensile properties, the diference between Process A and Process B was not clearly identified, however, it is understand that from the S-N diagram of fatigue result indicates the improvement in fatigue life of specimens fabricated from Process A as compared with that of Process B. On the other hand, from the observation on morphology of each specimens, the fracture behavior of WPCs was not clearly observed, regardless to the MAPP amount. However, the surface roughness observation at higher and lower fatigue load denote a hint on determining the fracture behavior of WPCs material.

In Chapter IV, WPCs specimens with different weight fraction of wood fibers was prepared to investigate the influence of wood fibers amount on fatigue properties and its fatigue fracture behavior of WPCs was characterized from the fracture surface observation. From the this study, the tensile and fatigue properties of WPCs were enhanced by compounding the wood fibers up to 50 wt.%. The good interfacial adhesion between the wood flour and the PP matrix, as a result from the addition of coupling agent MAPP to the compound, plays an important role towards enhancing the properties of WPCs material. In addition, the dispersion of wood flours inside the PP matrix was improved through the double extrusion process. From the fatigue fracture surface observation, it was conclude that the fatigue damage mechanism of WPCs specimen was initially formed by a plastic deformation or micro-crack at specimen's surface area

and then continued to bring the crazing process toward the inside of the specimen until finally a catastrophic failure occurred.

In present study, the fatigue fracture behavior of PMCs was studied and characterized via both qualitative and quantitative analyses on the images results from the microscopic observation of fatigue fracture surface. From the analyses, it is conclude that there are two different types of fatigue fracture behaviors which lead to the initiation of premature failure of the nanoclay and wood fibers filled plastic composites; (1) larger scale of agglomerates and closer distance between the agglomerates cause the formation of microcracks that are coalescence and lead to a fatigue crack initiation, (2) crazing process at the matrix-rich area that is functioned like a crack, brings to the failure of the composite materials. Poor distribution of the fillers is expected and inevitable during the actual manufacturing process material in the industry. Thus, the effects of poor distribution of the fillers during the manufacturing process and several related consequences have been investigated and clarified in this study.

References

[1] Edited by F.C. Campbell, Fatigue and Fracture, Understanding the Basic, Chapter 9: Fatigue and Fracture of Ceramics and polymers, ASM International, Ohio, (2012), 327-375.

[2] S. S. Ray, M. Okamoto, Polymer/layered silicate nanocomposites: a review from preparation to processing, *J Prog Polym Sci*, 28, (2003), 1539-1641.

[3] C.N. Wu, T. Saito, S. Fujisawa, H. Fuzukumi, and A. Isogai, Ultrastrong and high gas-barrier nanocellulose / clay-layered composites, *J Biomacromolecules*, 13, (2012), 1927-1932.

[4] N. Yu, Z.H. Zhang, S.Y. He, Fracture toughness and fatigue life of MWCNT/epoxy composites, *J Mater Sci Eng*, A 494, (2008), 380-384.

[5] L. Wang, K. Wang, L. Chen, Y. Zhang, C. He, Preparation, morphology and thermal/mechanical properties of epoxy/nanoclay composite, *J Composites A*, 37, (2006), 1890-1896.

[6] L.S. Schadler, L.C. Brinson, W.G. Sawyer, Polymer nanocomposites: A small part of the story, *JOM* , 59(3), (2007), 53-60.

[7] Z. Xia, L. Riester, W.A. Curtin, H. Li, B.W. Sheldon, J. Liang, B Chang, J.M. Xu, Direct observation of toughening mechanism in carbon nanotube ceramic matrix composites, *Acta Metall*, 52, (2004), 931-944.

[8] B.Akbari, R. Bagheri, Deformation mechanism of epoxy/clay nanocomposite. *J Eur Poly*, 43, (2007), 782-88.

[9] N.A. Siddiqui, R.S.C. Woo, J.K. Kim, C.C.K. Leung, A. Munir, Mode I interlaminar fracture behavior and mechanical properties of CFRPs with nanoclay-filled epoxy matrix, *Compos Part A: Appl Sci Manuf.*, 38, (2007), 449-460.

[10] L. Danyadi, T. Janecska, Z. Szabo, G. Nagy, J. Moczo, B. Pukanszky, Wood Flour Filled Composites: Compatibilization and Adhesion, *J Comp Sci Tech*, 67, (2007), 2838-2846.

[11] V.N. Hristov, M.Krumova, St. Vasileva, G. H. Michler, Modified Polypropylene Wood Composites. II. Fracture, Deformation, and Mechanical Properties, *J Apply Polym Sci,* 92, (2004), 1286-1292.

[12] E. Perez, L. Fama, S.G. Pardo, M.J. Abad, C. Bernal, Tensile and Fracture Behavior of PP/Wood Flour Composites, *J Composites B,* 43, (2012), 2795-2800.

[13] Alireza Ashori, Wood-PLastic Composites as Promising Green-Composites for Automotive Industries!, *J Bioresource Technology*,99,(2008), 4661-4667.

[14] S.Y Leu, T.H Yang, S.F Lo, T.H Yang, Optimized material composition to improve the physical and mechanical properties of extruded wood-plastic composites (WPCs), *J cons build mat*, 29, (2012), 120-127.

[15] D.V. Osti de Moraes, R. Magnabosco, G.H.Bolognesi Donato, S.H. Prado Bettini, M.C. Antunes, Influence of loading frequency on the fatigue behaviour of coir fibre reinforced PP composite, *J Polymer testing*, 41, (2015), 184-190.

[16] S.Liang, P. Gning, L. Guillaumat, Properties evaluation of flax/epoxy composites under fatigue loading, *J IJ Fatigue*, 63, (2014), 36-45.

[17] M.N. Ichazo, C. Albano, J. Gonzalez, R. Perera, M.V. Candal, Polypropylene/wood flour composites: treatments and properties, *J Comp Struct*, 54, (2001), 207-214.

[18] Y. Xu, S. Van Hoa, Mechanical properties of carbon fiber reinforced epoxy/clay nanocomposites, *Compos. Sci. Technol.*, 68(3-4), (2008), 854–861.

[19] D. R. Paul, L. M. Robeson, Polymer nanotechnology: Nanocomposites, *Polymer (Guildf).*, 49(15), (2008), 3187–3204.

[20] A. A. Azeez, K. Y. Rhee, S. J. Park, and D. Hui, Epoxy clay nanocomposites – processing, properties and applications: A review, *Compos. Part B Eng.*, 45(1), (2013), 308–320.

[21] M. Chan, K. Lau, T. Wong, M. Ho, and D. Hui, Mechanism of reinforcement in a nanoclay/polymer composite, *Compos. Part B Eng.*, 42(6), (2011), 1708–1712.

[22] C.K. Lam, H. Cheung, K. Lau, L. Zhou, M. Ho, and D. Hui, Cluster size effect in hardness of nanoclay/epoxy composites, *Compos. Part B Eng.*, 36(3), (2005), 263–269.

[23] J. a. M. Ferreira, L. P. Borrego, J. D. M. Costa, and C. Capela, Fatigue behaviour of nanoclay reinforced epoxy resin composites, *Compos. Part B Eng.*, 52, (2013), 286–291.

[24] M. Esteves, a. Ramalho, J. a. M. Ferreira, and J. P. Nobre, Tribological and Mechanical Behaviour of Epoxy/Nanoclay Composites, *Tribol. Lett.*, 52(1), (2013), 1–10.

[25] R. Taylor, Interpretation of the Correlation Coefficient: A Basic Review, *J. Diagnostic Med. Sonogr.*, 6(1), (1990), 35–39.

[26] K. Wang, L. Chen, J. Wu, M. L. Toh, C. He, and A. F. Yee, Epoxy Nanocomposites with Highly Exfoliated Clay: Mechanical Properties and Fracture Mechanisms, *Macromolecules*, 38(3), (2005), 788–800.

[27] H. Ito, H. Hattori, T. Okamoto, M. T. Takatani, Physical Properties of Wood Plastic Composites with Wasted MDF, *J Wood Industry*, 64, (2009), 268-272.

[28] H. Ito, H. Hattori, M. Takatani, T. Okamoto, T. Endo, S. H. Lee, M. Fuji, M. Ago, Y. Imanishi, Effect of Fibrillation on the Performance of Wood-Plastic Composites with High Filler Content, *Sen'i Gakkaisi*, 67(1), (2011), 39-45.

[29] S. Migneault, A. Koubaa, f. Erchiqui, A. Chaala, K. englund, M.P. Wolcott, Effects of Processing Method and Fiber Size on the Structure and Properties of Wood-Plastic Composites, *J Composites A*, 40, (2009), 80-85.

Acknowledgements

Bismillah ir-Rahman ir-Rahim. In the name of Allah, the Most Gracious, the Most Merciful. *Alhamdulillah*. All praises and thanks belong to Allah.

This study had been carried out at the Graduate School of Science and Engineering in Yamaguchi University from October 2012 to September 2015. I owe my deepest gratitude to my supervisor, Professor Dr. Koichi Goda, for his inspiring and inexhaustible support during all these years. His wide knowledge and energy have been enormously valuable for the project. In addition, his enthusiasm and willingness to help are also very much appreciated. Not forgetting Associate Professor Dr. Junji Noda, to whom I would like to extend my warmest thanks for his generous help and friendly support throughout the study. I also wish to extend my appreciation to all fellow friends in the laboratory.

To the staff of Centre of Instrumental Analysis, Yamaguchi University, Mr. Yoji Morifuku, I cannot thank you enough for the guidance and technical supports on the elemental analysis for the study.

Herein, I am pleased to mention that I had garnered enormous support from HUNTSMAN Co., Ltd which had made the Araldite AY103-1, Hardener HY956 and mold lubricant available for this study. I also would like to thank the Nanocor Inc. for kindly guiding me on the processing method of the nanoclay and providing the nanomer ®nanoclay I.28E for this study. I would also like to express my gratitude towards Mr. Hirozaki Ito and TOCLAS

Corp., for their willingness to assist and guide me in discovering the new knowledge and experiences on WPCs material.

In addition, a warm thank you to all the staff of Faculty of Mechanical Engineering, Universiti Teknikal Malaysia Melaka (UTeM) for the excellent supports and insightful advice during the study in Japan. It is a pleasure to acknowledge with gratitude the financial support by the Ministry of Education Malaysia, which has made the completion of this study possible. Thank you very much.

Finally, I wish to express my loving thoughts and gratitude to my parents, Nordin bin Awang Ngah and Zaidah binti Mohd Taib, for their never ending encouragement and heartening supports during my ups and downs throughout the study. I would also to give my special thanks to all my siblings, Yuhana, Dasima, Mohd Nor Amin, Norfiza, and Syahida for listening, offering me advice, and supporting me through this entire process. Not forgetting, my special thanks to all my fellow friends in Japan and also to all Malaysian's brothers and sisters in Yamaguchi University for their helps and generous support during this study. *Terima kasih*.